Moisture Interchange between Clouds and Environment in a Tropical Atmosphere

by

Carlos S. López Carrillo

Submitted in Partial Fulfillment of the Requirements
for the Degree of

Doctor of Philosophy

Physics Department

New Mexico Tech

Socorro, New Mexico

July 2001

To Julieta, Lucio, and Damián

The best children no father could have.

abstract

In this work a theory for moisture interchange between cloud systems and their environment in the tropical atmosphere is developed. Data collected during the intensive operation period of TOGA-COARE (Tropical Ocean and Global Atmosphere–Coupled Ocean-Atmosphere Response Experiment) is then used to study, on a case-by-case basis, the nature of this interchange for different convective regimes. The kinematic characteristics of the studied systems for each of the ten cases are synthesized from Doppler measurements made by the two National Oceanic and Atmospheric Administration WP-3D aircraft, while the environmental conditions were retrieved from balloon soundings made nearby the studied region. For this ten-case sample, a strong correlation between system-top height and tropospheric moisture (in the layer between 1 and 10 km) is found. The analysis indicates that it is tropospheric moisture which is controlling the height of the clouds and not vice-versa. It is found that the role of small clouds is to moisten the environment while deep convective regimes dry their environment.

Acknowledgments

At the end of the long period of time, that the making of a dissertation spans, it is good to look back and see the team of people that had helped you, so you can accomplish this goal. It is good to know that one is not alone. At this point, I would like to thank some of the many people that had helping me in various ways.

I want to thank the guidance and support that I received from my adviser Dr. David J. Raymond, who expended with me many hours discussing how convection works in general, and in particular over the tropical regions. I also want to thank the confidence deposited in me by Dr. Odon Sanchez, who first told me about the research opportunities in atmospheric sciences, and for his support that allow me to pursue further graduate studies in this area. I'm grateful to the members of my committee: Drs. Kenneth R. Mischwaner, Steve Schaffer, and Ken Eack for their prompt review of the manuscript and the suggestions they made to improve it. I particularly want to thank my fellow student Clifton Murray for proof reading the many versions of the manuscript, which considerably improved the way it was written. Special thanks goes to Sandy Kieft whose mastery and efficiency of administrative matters, took lots of worries from my head.

A good part of this work could not be possible with out the data provided by John Daugherty from NOAA/NSSL. Most of the data analysis was made using the in-house CANDIS software pioneered by David J. Raymond and further developed by many students here at New Mexico Tech. I also benefited from powerful packages such as Rlab by Ian Searle, and Gri by Dan E. Kelley. All my work was done on a Linux-debian platform.

I especially want to thank my source of continuous inspiration since I remember – my mother, who instilled in me her strong work ethic. My children, I have to thank no only for being a source of inspiration for me, but also for being so patient with me and give up much of our precious time together.

From all people that had helped me, there is one for who I can hardly express my gratitude, for supporting me in so many ways, for being the source of energy and joy that keep me going ... Thank You, Chata – my wife.

This work was supported by the following National Science Foundation grants: ATM-9311735, ATM-9413289, ATM-9616290, and ATM-0082612.

Contents

List of Figures

List of Tables

Introduction

In the tropics several convective regimes, ranging from suppressed to deep convection, can be found (Johnson et al. 1992). The study of these regimes is important not only for increasing our knowledge about their internal dynamics and evolution, but also for understanding the atmospheric circulations in which they are embedded. For instance, shallow convection and stratiform clouds can have a strong effect on radiative transfer; deep convective cores, on the other hand, can dominate the thermodynamic structure of the atmosphere via the latent heat release associated with their precipitation.

Although many ideas have been proposed, determining where and when a particular kind of convection is going to occur is still an unsolved problem. The Boundary Layer Quasi-equilibrium theory (BLQ) of moist convection developed by Emanuel (1994) and Raymond (1995) addresses, at least partially, the question of how moist convection is regulated over tropical oceans. In this theory, convection appears to be initiated when the mean value of moist entropy in the boundary layer exceeds a certain threshold. However, the kind of convection is thought to depend on mid-level conditions in a way that is not well understood. Particularly, mid-level relative humidity is believed to play a crucial role for the outcome convection. In this picture, a dry mid-level atmosphere corresponds to a very suppressed condition for convection. If the threshold value of boundary layer moist entropy is reached, then the main function of convection is to start moistening the atmosphere, so shallow convection may occur. Once the middle atmosphere becomes moist, convection can go deep. In this case, huge amounts of latent heat are released due to precipitation formation that takes place in the convective cores. In the stratiform region, however, things go

differently. Since precipitation tends to evaporate if the atmosphere is not saturated, evaporation from falling stratiform particles tends to cool down this region, which in turn promotes downdrafts. By this mechanism, low values of moist entropy are injected into the boundary layer so its value is brought back below the threshold for convection. Then, the next convection event has to wait until the surface fluxes of moist entropy are able to recharge the boundary layer. In short, the hypothesis boils down to an equilibrium between the surface fluxes and downdraft fluxes of moist entropy, where downdrafts are modulated by mid-level moisture. Although BLQ theory does not predict the kind of convection for a given environment, it does suggest a link between mid-level moisture and type of convection. There are indeed some observational studies, based primarily on sounding arrays, that suggest the importance of the mid-level moisture in determining the outcome of the convection (Brown and Zhang, 1997; Sherwood, 1999).

In this study, we will not attempt to test the basic hypothesis of BLQ. Rather, we will try to shed some light on the role played by the tropospheric moisture on the characteristics of convection once it has been initiated. We use data from 10 case studies observed during the intensive operation period of TOGA-COARE (Tropical Ocean and Global Atmosphere–Coupled Ocean-Atmosphere Response Experiment) to address the following questions: First, is there a reasonable correlation between cloud top and environmental moisture present on a case-by-case basis? Second, what is the nature of the moisture interchange between clouds and environment – is the environment humid simply because we have bigger clouds that are moistening it? Or do clouds grow larger because the environment is already moistened? In particular, we

try to understand the role of different convective regimes in this moisture interchange.

While the correlation between cloud top and tropospheric moisture is addressed directly from the data analysis, the study of the moisture interchange requires a more involved approach. In part one, we describe in detail this approach, which basically consists in estimating the time rate of change of moist entropy and moist energy for each case study. The concepts of moist energy and entropy are so fundamental to our research that we explore how they are defined, how their governing equations are obtained, and under which circumstances the budget equations of these variables can be used to address the moistening or drying tendencies in the tropical atmosphere. In part two, the preparation of sounding and radar data is presented first, followed by the results obtained from those data. Conclusions are offered after part two. Since the radar data analysis is central to this research and it is studied so extensively, we believe that it deserves a full chapter. However, with the aim of keeping the focus on the main purpose of this work, this chapter is offered as appendix B. We also include a series of other appendices that support derivations and results.

Part I

Fundamental Equations

As mentioned in the introduction, the main goal in this work is to understand how convective clouds over the oceans moisten or dry their environment. A direct approach to this problem is to analyze the budget equation of water substance, but we show that the moistening or drying depends upon, among other things, good estimates of precipitation. This fact precludes taking the direct approach, because errors in the estimation of precipitation are as large as 50%. Thus, we must choose an indirect approach toward this problem. The approach taken here is based on the following assumption about the atmosphere: If horizontal temperature gradients are small and vertical temperature profiles do not change much with time, then the mass-weighted average of the energy and entropy depend only on the amount of water in the atmosphere, and their maximum values are attained when the atmosphere becomes saturated. Thus, an increase in the average values of energy and entropy indicates moistening of the environment. In the deep tropics, horizontal and temporal gradients of temperature are very small, so this approach is justified. Therefore in this part, we derive expressions for the energy and entropy of a precipitating atmosphere, and their evolution equations. We combine the budgets for energy, entropy, and water to obtain equations which do not depend on precipitation. Then we show that even when the modified equations for energy and entropy still contain unknown sources, they can be used to study the moistening or drying tendencies in the environment due to convective clouds.

We consider the atmosphere as a multicomponent fluid whose components can flow relative to each other. Although we have included precipitation and cloud condensate as a part of this fluid, we follow the same formalism that is used to describe

inhomogeneous mixtures of gases (de Groot and Mazur, 1962). Therefore, the relative motion between condensate and mean flow is described as a diffusive motion. This approach allows for a more accurate account of energy and entropy budgets, because it has the great advantage of considering drag forces as internal forces.

We assume that the atmosphere is composed of dry air, water vapor, cloud droplets, cloud ice, liquid water precipitation, and ice precipitation. However, we consider that cloud condensate is liquid below the freezing level, while above the freezing level it is ice. Therefore, super-cooled droplets are not taken into account. While this is an important issue in cloud microphysics, we assume that it does not have a big impact on the overall budgets of the atmosphere. We assume that dry air, water vapor and cloud condensate all have the same temperature, while various forms of precipitation (ice, liquid or both) may have different temperatures.

The governing equations are derived by considering the budget of each variable inside a fixed, but otherwise arbitrary, control volume. Once the governing equations are obtained, we average them over a particular control volume.

Our final budget equations are restricted to the case where the precipitation that reaches the surface is purely liquid water. This simplification, which is quite reasonable for tropical regions, allows the elimination of all influence of the precipitation from the budget equations. This fact is particularly important as precipitation is one of the more poorly estimated variables in the budgets.

Chapter 1

Multicomponent fluids

Since our system is composed of dry air and water, it is a multicomponent fluid. We will regard the different water phases as different components in the fluid. Furthermore, we consider precipitation and cloud condensate as different components, even when they correspond to the same water phase.

In multicomponent fluids, one of the important parameters is the relative concentration of each of the components. We define concentration in terms of mass fractions. For instance, if in a fixed volume we have a total mass M, and the contribution to this total mass due to the jth component is m_j, then the concentration of the jth component is given by

$$q_j = \frac{m_j}{M} \tag{1.1}$$

The partial density is defined simply as

$$\rho_j = \frac{m_j}{V} \tag{1.2}$$

where V is the volume that contains the total mass, M.

Since the total mass is simply the sum of all masses from all components, the total density may be defined as

$$\rho = \frac{1}{V}\sum_j m_j \tag{1.3}$$

$$= \sum_j \rho_j \tag{1.4}$$

In general, all components may move relative to each other. However, as a whole, the fluid moves with some mean velocity. The center-mass velocity of a multicomponent fluid is defined as the mass-weighted average of the velocities of each of the fluid's components:

$$\mathbf{v} = \frac{1}{\rho}\sum_j \rho_j \mathbf{v}_j \tag{1.5}$$

where ρ is the total density of the fluid, and the summation is over all fluid's components.

The difference between the center-mass velocity and the velocity of a fluid's component gives rise to the concept of diffusive velocity, which is normally used in the description of heterogeneous gas mixtures. In our case however, we find it more useful to define the diffusive velocities not with respect to the center-mass velocity, but with respect to the dry air mean velocity. Nevertheless, the formalism remains the same. Hence, the velocity of the jth component of the mix can be written as

$$\mathbf{v}_j = \mathbf{v}_d + \mathbf{v}_{Dj} \tag{1.6}$$

where $\mathbf{v}_d$ is the mean velocity of dry air, and $\mathbf{v}_{Dj}$ is the diffusive velocity of the jth component with respect to the dry air flow.

Similar to the center-mass velocity and total density, it is possible to define average values for each *intensive parameter* of a multicomponent fluid. Call χ_j the value of

some parameter associated with the jth component in the mix. Then the mean value of that parameter, associated with the fluid as a whole, is defined as the mass-weighted average over all components of the mix:

$$\chi = \frac{1}{\rho} \sum_j \rho_j \chi_j \tag{1.7}$$

where ρ is the total density. Also, with every intensive parameter in a substance, we can associate a *density parameter* given simply by the product of the intensive parameter and the mass density of the substance. So, if χ_j is the intensive parameter associated with the jth component and ρ_j is the mass density of such component, then the associated density parameter is given by

$$\psi_j = \rho_j \chi_j \tag{1.8}$$

The concept of density parameter is very useful in defining fluxes of intensive parameters that arise due to the flow of matter. For instance, vapor flux can carry energy, entropy, and momentum. If χ_j is one of the intensive parameters in our mix, then the flux of this quantity due to the flux of the jth component of the fluid is defined as the product of the associated density parameter with the velocity of the fluid component, that is,

$$\mathbf{J}_j = (\rho_j \chi_j)\mathbf{v}_j \tag{1.9}$$

and the total flux of χ_j due to all mass transports is

$$\mathbf{J} = \sum_j [(\rho_j \chi_j)\mathbf{v}_j] \tag{1.10}$$

where the summation is over all components that make up the flux of mass. It will be convenient to write this kind of flux as composed of two parts: convective and

diffusive. Using equations (1.6) and (1.7), we can write

$$\begin{aligned} \mathbf{J} &= \sum_j \rho_j \chi_j (\mathbf{v}_d + \mathbf{v}_{Dj}) && (1.11) \\ &= \mathbf{v}_d \sum_j \rho_j \chi_j + \sum_j \rho_j \chi_j \mathbf{v}_{Dj} && (1.12) \\ &= \rho \chi \mathbf{v}_d + \mathbf{D}_\chi && (1.13) \end{aligned}$$

where we have defined $\mathbf{D}_\chi$ as the diffusive flux of χ.

Chapter 2

Standard techniques

In this chapter we present a standard technique used to derive the governing equation in flux form of an intensive variable. In this technique, we first write a budget equation in integral form for our variable, and then we use some mathematical properties to extract the differential governing equation corresponding to the budget.

Writing down the budget equation is the most important part. It is where we apply all the physics we know about the problem. The extraction of the differential governing equation is a mathematical problem. We will call this mathematical part "the standard fixed-control-volume technique."

2.1 Budget balance

In order to write down the budget balance, we use the Eulerian approach in which we consider the budget in a fixed control volume. Let's call ψ_j the amount per unit volume (density) of some property in the fluid associated with component j of the

fluid. (Keep in mind that here density means density parameter, see equation 1.8.) The total amount of this property in the control volume, V, is simply

$$\Psi_j = \int_V \psi_j \; dV \tag{2.1}$$

Since the control volume is fixed in space, the total change in Ψ_j is due to the net flux through the control volume walls plus any sources and sinks of ψ_j inside the volume. Calling $\mathbf{J}_j$ the net flux of ψ_j, and $\mathcal{S}_j$ its net source per unit volume, the budget equation is given by

$$\frac{d}{dt}\int_V \psi_j \; dV = -\oint_A \mathbf{J}_j \cdot \hat{\mathbf{n}} \; da + \int \mathcal{S}_j \; dV \tag{2.2}$$

where the closed-area integral is taken over the surface of the control volume V, and the unit vector $\hat{\mathbf{n}}$ is the outward-pointing normal to such surface. The minus in front of the closed integral is due to the convention of defining the normal vector, $\hat{\mathbf{n}}$, as going out of the volume.

2.2 Standard fixed-control-volume technique

Once we have the budget equation, the governing equation is obtained as follows: we apply the Gauss's theorem to the surface integral in the budget equation. The total time derivative is introduced inside the integral as a partial derivative. This is possible because the control volume is fixed in time. Therefore, the budget equation can be written as a single volume integral

$$\int_V \left(\frac{\partial \psi_j}{\partial t} + \boldsymbol{\nabla} \cdot \mathbf{J}_j - \mathcal{S}_j \right) \; dV = 0 \tag{2.3}$$

Although the control volume is fixed, it is arbitrary. Hence, the equation must be satisfied for any value of such volume, even in the limit where the control volume goes to zero. This implies that the integrand itself must be zero, which leads to the differential governing equation associated with the original budget of ψ_j:

$$\frac{\partial \psi_j}{\partial t} + \boldsymbol{\nabla} \cdot \mathbf{J}_j = \mathcal{S}_j \tag{2.4}$$

This technique will be used frequently through this part when deriving governing equations for mass, linear momentum, energy, and entropy. The main challenge will be in carefully writing the fluxes and sources for each case.

Chapter 3

Governing equations

3.1 Mass Continuity

Here we present the derivation of the mass continuity equation for the jth component in our fluid.

Call ρ_j the density of the jth component of the fluid and $\mathbf{v}_j$ the mean velocity of the particles of this component. So, the net mass flux due to the jth component can be written as

$$\mathbf{J}_j = \rho_j \mathbf{v}_j \tag{3.1}$$

Therefore, the mass budget in an Eulerian control volume can be written as

$$\frac{d}{dt}\int_V \rho_j \; dV = -\oint_S \rho_j \mathbf{v}_j \cdot \hat{\mathbf{n}} \; da + \int_V \mathcal{S}_j \; dV \tag{3.2}$$

where the closed-area integral is taken over the surface of the volume V. The quantity $\mathcal{S}_j$ is the mass source of the jth component per unit volume. This equation basically says that the increase of the total mass of the jth component inside the volume V

is due to the inflow of the component into the volume, plus any additional source of this component. In the case of water vapor, for instance, the source may represent the conversion between water vapor and condensate.

Using the standard fixed-control-volume technique (see section 2.2), the differential governing equation for the mass of the jth component in our mix is given by

$$\frac{\partial \rho_j}{\partial t} + \boldsymbol{\nabla} \cdot (\rho_j \mathbf{v}_j) = \mathcal{S}_j \tag{3.3}$$

3.2 Dry air

Since in our atmosphere dry air is not created, destroyed, or converted into anything else, its source per unit mass is zero; which leads to the following mass conservation equation for dry air:

$$\frac{\partial \rho_d}{\partial t} + \boldsymbol{\nabla} \cdot (\rho_d \mathbf{v}_d) = 0 \tag{3.4}$$

From now on, we use the subindex d to represent dry air properties, only.

3.3 Individual components of water substance

For each individual component of the water substance in our atmosphere, the source term is different. For instance, since water substance is neither created nor destroyed in our system, but simply transformed among its different phases, the sources for each of the water components can be considered simply as the rates of conversion per unit mass among those phases. All possible transformations among those phases are

listed below:

$Source$	$from$	$into$
$\mathcal{S}_{cl\to v}$	cloud – liquid water	water vapor
$\mathcal{S}_{cl\to ci}$	cloud – liquid water	cloud ice
$\mathcal{S}_{cl\to pi}$	cloud – liquid water	ice precipitation
$\mathcal{S}_{cl\to pl}$	cloud – liquid water	precipitation – liquid water
$\mathcal{S}_{pl\to v}$	precipitation – liquid water	water vapor
$\mathcal{S}_{pl\to ci}$	precipitation – liquid water	cloud ice
$\mathcal{S}_{pl\to pi}$	precipitation – liquid water	ice precipitation
$\mathcal{S}_{ci\to v}$	cloud ice	water vapor
$\mathcal{S}_{ci\to pi}$	cloud ice	ice precipitation
$\mathcal{S}_{pi\to v}$	ice precipitation	water vapor

In all cases, a negative value of those rates would imply that the opposite transformation is taking place.

As an example, the total source for precipitating ice can be written as

$$\mathcal{S} = \mathcal{S}_{cl\to pi} + \mathcal{S}_{pl\to pi} + \mathcal{S}_{ci\to pi} - \mathcal{S}_{pi\to v} \tag{3.5}$$

3.4 Total water substance

In general, estimating rates of conversion among different phases of water is a very difficult task. Fortunately, the net source for total water inside any control volume is zero, because water is just transformed among the different phases. Therefore, the budget of total water substance in an arbitrary fixed control volume is reduced to the

balance between the increase in total mass of water inside the volume and the inflow of the different water components. In this case, the net flux of water is obtained by adding the fluxes for all water components. If ρ_j and $\mathbf{v}_j$ are the density and velocity for the jth component of water substance, then the flux of water from the control volume is given by $\mathbf{J}_w = \sum_j \rho_j \mathbf{v}_j$ where the summations extend only through the water components.

Defining the total water density as

$$\rho_w = \sum_j \rho_j \tag{3.6}$$

and using equation (1.13), the total flux of water can be written in terms of its convective and diffusive components as $\mathbf{J}_w = \rho_w \mathbf{v}_d + \mathbf{D}_w$, where $\mathbf{v}_d$ is the mean velocity of dry air, and $\mathbf{D}_w = \sum_j \rho_j \mathbf{v}_{Dj}$ is the diffusive flux of water substance. Therefore, the budget equation can be written as

$$\frac{d}{dt}\int_V \rho_w \; dV = -\oint_S (\rho_w \mathbf{v}_d + \mathbf{D}_w) \cdot \hat{\mathbf{n}} \; da \tag{3.7}$$

Applying the standard fixed-control-volume technique (see section 2.2), we arrive at the following continuity equation for water substance in flux form

$$\frac{\partial \rho_w}{\partial t} + \boldsymbol{\nabla} \cdot (\rho_w \mathbf{v}_d + \mathbf{D}_w) = 0 \tag{3.8}$$

The continuity equation for total water will become very important in the derivation of our final energy and entropy budget equations.

3.5 Total Mass

Since neither the total water substance nor dry air have net sources, by using the same arguments as in the previous section we can write the total mass continuity equation for the atmosphere as

$$\frac{\partial \rho}{\partial t} + \boldsymbol{\nabla}\cdot(\rho \mathbf{v}) = 0 \tag{3.9}$$

where we have used the definitions of total density (equation 1.4) and center-mass velocity (equation 1.5). Using equation (1.6), the center mass velocity can be written in terms of the dry air and diffusion velocities as follows,

$$\mathbf{v} = \mathbf{v}_d + \frac{1}{\rho}\sum_j \rho_j \mathbf{v}_{Dj} \tag{3.10}$$

Therefore in terms of the dry air mean velocity, the total mass continuity equation takes on the form

$$\frac{\partial \rho}{\partial t} + \boldsymbol{\nabla}\cdot(\rho \mathbf{v}_d) = -\boldsymbol{\nabla}\cdot\mathbf{D}_\rho \tag{3.11}$$

where we have defined

$$\mathbf{D}_\rho = \sum_j \rho_j \mathbf{v}_{Dj} \tag{3.12}$$

as the diffusive mass flux.

3.6 Linear Momentum equation

Call ρ_j and $\mathbf{v}_j$ the density and velocity of the jth component of the fluid. The density of momentum associated with the component is $\rho_j \mathbf{v}_j$. Therefore, the flux of linear

momentum due to mass transport is given by the tensor

$$\overleftrightarrow{\mathrm{M}} = \sum_j [(\rho_j \mathbf{v}_j)\mathbf{v}_j] \tag{3.13}$$

Hence, the budget equation for the total momentum inside a fixed-control volume can be written as

$$\frac{d}{dt}\int_V \sum_j \rho_j \mathbf{v}_j \; dV = -\oint_S \overleftrightarrow{\mathrm{M}} \cdot \hat{\mathbf{n}} \; da + \mathcal{F} \tag{3.14}$$

where the summation is over all components of the mix. The source term, $\mathcal{F}$, represents all forces acting over the fluid in our control volume. Generally speaking, there are two kinds of forces: body forces and surface forces. Body forces may act on every bit of matter inside the control volume and are therefore characterized by their strength per unit mass. On the other hand, surface forces just act at the boundaries of the control volume and they are characterized by a stress tensor. Call $\mathbf{B}_j$ the body force per unit mass acting on component j, and $\overleftrightarrow{\mathrm{T}}$ the stress tensor. The sources of momentum can be written as

$$\mathcal{F} = \oint_S \overleftrightarrow{\mathrm{T}} \cdot \hat{\mathbf{n}} \; da + \int_V \sum_j \rho_j \mathbf{B}_i \; dV \tag{3.15}$$

where the summation extends through all components of the fluid. Therefore, the budget equation becomes

$$\frac{d}{dt}\int_V \rho \mathbf{v} \; dV = -\oint_S \overleftrightarrow{\mathrm{M}} \cdot \hat{\mathbf{n}} \; da + \oint_S \overleftrightarrow{\mathrm{T}} \cdot \hat{\mathbf{n}} \; da + \int_V \sum_j \rho_j \mathbf{B}_j \; dV \tag{3.16}$$

where the definition of the center-mass velocity (eq. 1.5) has been used.

Now, applying the standard fixed-control-volume technique (see section 2.2) the governing equation for linear momentum in flux form is

$$\frac{\partial(\rho \mathbf{v})}{\partial t} + \boldsymbol{\nabla} \cdot \overleftrightarrow{\mathrm{M}} = \boldsymbol{\nabla} \cdot \overleftrightarrow{\mathrm{T}} + \rho \mathbf{B} \tag{3.17}$$

where we have defined the net body force per unit mass as

$$\mathbf{B} = \frac{1}{\rho} \sum_j \rho_j \mathbf{B}_i \tag{3.18}$$

3.7 Total energy equation

The total energy per unit mass of the fluid is defined as the mass-weighted sum of the specific energies of all components of the fluid

$$e = \frac{1}{\rho} \sum_j \rho_j e_j \tag{3.19}$$

where ρ is the total density of the fluid. The total energy for each of the components is in turn composed of the sum of internal (u), kinetic (k) and potential (ϕ) energies

$$e_j = u_j + k_j + \phi_j \tag{3.20}$$

In order to write the budget equation for the total energy, we need to be able to identify all forces that can do work on our system as well as all energy fluxes through the boundary of the control volume.

Since the total energy of the fluid includes the potential energy, all conservative forces that make up such potential do not enter into our budget. This is because conservative forces only redistribute energy between potential and kinetic energy. We will assume that all body forces acting on our fluid are conservative and that their effects are accounted for in the potential energy term. Internal forces (like drag between condensate and gas) do not need to be included, because they only redistribute energy among its different forms, therefore they do not change the total

value of energy in our volume. Forces that do not do any work on the system, like the Coriolis force, also can be ignored in our analysis. On the other hand, surface forces acting over the periphery of our volume constitute an important interaction between our system and its environment. These forces include dissipative and non-dissipative effects. They are represented by the stress tensor, which for Newtonian fluids is given by

$$\overleftrightarrow{\mathrm{T}} = -P\overleftrightarrow{\mathrm{I}} + \overleftrightarrow{\nu} \tag{3.21}$$

where P is the thermodynamic pressure, $\overleftrightarrow{\mathrm{I}}$ the identity tensor, and $\overleftrightarrow{\nu}$ the viscous stress tensor. The power associated with these forces is

$$\oint (\overleftrightarrow{\mathrm{T}} \cdot \mathbf{v}) \cdot \hat{\mathbf{n}} \; da \tag{3.22}$$

where $\mathbf{v}$ is the center-mass velocity of the flow.

Besides forces doing work on the fluid, energy can leave or enter the system through its walls. Heat conduction, plus wave and mass transport are the possible mechanisms. Radiative heat on the other hand, may travel beyond the physical boundary of the system before interacting with the system's matter. So, this mechanism of energizing the system is regarded as a source of energy.

Call $\mathbf{J}_R$ the radiative flux at any location. Then the source of radiative energy per unit volume is defined as the convergence of the radiative flux, $-\boldsymbol{\nabla}\cdot\mathbf{J}_R$. Hence the total radiative source of energy is given by

$$-\int_V \boldsymbol{\nabla}\cdot\mathbf{J}_R \; dV \tag{3.23}$$

Note that the integration over a volume V is, by the Gauss's theorem, mathematically equivalent to the radiative flux of energy passing through the physical boundary of

this volume. Nevertheless, regarding the radiation as a source has the conceptual advantage of explicitly excluding the radiation field from the system.

Returning to the exchange mechanisms, atmospheric waves travel in and out of the control cylinder and they transport energy as they move. Even though in the atmosphere there are a variety of waves (sound waves, gravity waves, Rossby waves, etc.), we define $\mathbf{J}_W$ as the flux of energy through the control volume due to any wave transport. Hence the net flux of energy due to atmospheric wave transport is given by

$$-\oint \mathbf{J}_W \cdot \hat{\mathbf{n}} \; da \tag{3.24}$$

Note that when waves move in or out of the control volume, they must cross the boundary. Therefore their effect, regarding energy transfer, could be accounted for in the power associated with the stresses at the boundary of the control volume. However, we have decided to exclude wave transport from the other energy transfers taking place at the boundary, such as steady motion of the boundary, or dissipation at the boundary. In this sense the velocity fields, and the thermodynamic pressure, we are using in this work, do not include the variations associated with wave transport phenomena.

The heat conduction mechanism can also be accounted for by defining the flux of conductive heat through the control volume. Calling this flux $\mathbf{J}_C$, the total heating rate for the volume can be written as

$$-\oint \mathbf{J}_C \cdot \hat{\mathbf{n}} \; da \tag{3.25}$$

Finally, the net flux of energy due to mass transport through the surface that encloses

the control volume is given by

$$-\oint \sum_j \rho_j e_j \mathbf{v}_j \cdot \hat{\mathbf{n}}\ da \tag{3.26}$$

Using equation (3.19), and (1.13) this can be written in terms of convective and diffusive fluxes as

$$-\oint (\rho e \mathbf{v}_d + \mathbf{D}_e) \cdot \hat{\mathbf{n}}\ da \tag{3.27}$$

where $\mathbf{v}_d$ is the mean velocity of dry air and

$$\mathbf{D}_e = \sum_j \rho_j e_j \mathbf{v}_{Dj} \tag{3.28}$$

is the diffusive flux of energy.

Collecting all the contributions, the energy budget equation can be written as follows:

$$\begin{aligned} \frac{d}{dt}\int_V \rho e\ dV = &- \oint (\rho\, e\, \mathbf{v}_d + \mathbf{D}_e) \cdot \hat{\mathbf{n}}\ da \\ &- \oint \mathbf{J}_C \cdot \hat{\mathbf{n}}\ da - \oint \mathbf{J}_W \cdot \hat{\mathbf{n}}\ da \\ &+ \oint (\overleftrightarrow{\mathrm{T}} \cdot \mathbf{v}) \cdot \hat{\mathbf{n}}\ da - \int_V \boldsymbol{\nabla}\cdot\mathbf{J}_R\ dV \end{aligned} \tag{3.29}$$

Now using the standard fixed-control-volume technique (section 2.2), it follows that the governing equation for the total energy in flux form is

$$\frac{\partial(\rho e)}{\partial t} + \boldsymbol{\nabla}\cdot(\rho\, e\, \mathbf{v}_d + \mathbf{D}_e + \mathbf{J}_R + \mathbf{J}_C + \mathbf{J}_W - \overleftrightarrow{\mathrm{T}} \cdot \mathbf{v}) = 0 \tag{3.30}$$

Assuming that our fluid can be regarded as a Newtonian fluid, the governing equation may be written as

$$\frac{\partial(\rho e)}{\partial t} + \boldsymbol{\nabla}\cdot(\rho\, e\, \mathbf{v}_d + \mathbf{D}_e + P\mathbf{v} + \mathbf{J}_R + \mathbf{J}_C + \mathbf{J}_W - \overleftrightarrow{\nu} \cdot \mathbf{v}) = 0 \tag{3.31}$$

where $\mathbf{v}$ is the center-mass velocity.

In order to obtain a more succinct expression for the energy governing equation, we use the relation between center-mass and dry-air velocities (equation (3.10)) and the definition of the diffusive flux of energy (equation (3.28)) to make the following rearrangements:

$$\begin{aligned}
\rho\, e\, \mathbf{v}_d + \mathbf{D}_e + P\mathbf{v} &= \rho\, e\, \mathbf{v}_d + P\left[\mathbf{v}_d + \frac{1}{\rho}\sum_j \rho_j \mathbf{v}_{Dj}\right] + \sum_j \rho_j e_j \mathbf{v}_{Dj} \\
&= \rho(e + P/\rho)\mathbf{v}_d + \sum_j [(\frac{\rho_j}{\rho})P + \rho_j\, e_j]\mathbf{v}_{Dj} \\
&= \rho(e + P\alpha)\mathbf{v}_d + \sum_j (P_j + \rho_j\, e_j)\mathbf{v}_{Dj} \\
&= \rho(e + P\alpha)\mathbf{v}_d + \sum_j \rho_j(e_j + P_j\alpha_j)\mathbf{v}_{Dj} \qquad (3.32)
\end{aligned}$$

where α and α_j are the specific volumes for the fluid as a whole and its jth component, respectively. Using the definition of enthalpy and total internal energy, we can show that $e_j + P_j\alpha_j$ is the Bernoulli function of the jth component. That is,

$$\begin{aligned}
e_j + P_j\alpha_j &= (u_j + P_j\alpha_j) + k_j + \phi_j \\
&= h_j + k_j + \phi_j \\
&= b_j \qquad (3.33)
\end{aligned}$$

where

$$h_j = u_j + P_j\alpha_j \qquad (3.34)$$

is the enthalpy of the jth component of the fluid. Hence, in analogy to the total energy, the Bernoulli function for the system can be defined as

$$b = \frac{1}{\rho}\sum_j \rho_j b_j \qquad (3.35)$$

which can be simplified to

$$b = e + P\alpha \tag{3.36}$$

Now using the definition of the Bernoulli function for the system and its components, the governing equation for energy can be written as

$$\frac{\partial(\rho e)}{\partial t} + \boldsymbol{\nabla}\cdot(\rho\, b\, \mathbf{v}_d + \mathbf{J}_R + \mathbf{J}_C + \mathbf{J}_W + \mathbf{D}_b - \overleftrightarrow{\nu}\cdot\mathbf{v}) = 0 \tag{3.37}$$

where we have defined the diffusive flux of b as

$$\mathbf{D}_b = \sum_j \rho_j b_j \mathbf{v}_{Dj} \tag{3.38}$$

3.8 Entropy

Normally in thermodynamics, the entropy is defined only for systems in thermodynamic equilibrium. For example, a system in which the three phases of water are present would not normally have an entropy defined for it, except of course at the triple point, where all water phases are in equilibrium with each other. For the case in which only two phases of water are present at the same temperature, then in order to assign an entropy to such a system, it would need to be saturated with respect to either ice or water, depending on what the two coexisting phases are. In spite of that, we will use the concept of local thermodynamic equilibrium (Callen, 1960) to define a local entropy for any infinitesimal region of a non-equilibrium system. Based on this concept, the functional dependence of the local entropy on the local extensive parameters (volume, energy, etc.) is by definition taken to be the same as such dependence in equilibrium. The assumption of local thermodynamic equilibrium

also implies that the functional dependence of the intensive parameters (temperature, pressure, etc.) on the local extensive parameters is the same as that for equilibrium. (It is this last condition that allows us, for instance, to speak of the temperature varying continuously throughout a piece of material, despite the fact that temperature itself is normally defined only for equilibrium systems.)

A system that is not in equilibrium will evolve until it reaches its equilibrium state. For example, a closed system composed of water vapor and liquid water at the same temperature is not in equilibrium unless the water vapor is saturated with respect to water. Such a non-equilibrium system will be driven to equilibrium by evaporation of the liquid water. This evaporation will act as a source of entropy, increasing the entropy until the system reaches saturation. So in general, the entropy for non-equilibrium systems will be governed by a tendency equation that tells us how the entropy is evolving. In this section, we develop the governing entropy equation in its flux form for our system.

The entropy per unit mass of a multicomponent system is defined as the mass-weighted sum of the specific entropies of the components

$$s = \frac{1}{\rho} \sum_j \rho_j s_j \tag{3.39}$$

Therefore, the change of the total entropy inside a control volume is

$$\frac{d}{dt} \int_V \rho s \ dV \tag{3.40}$$

In the theory of irreversible processes, this change in entropy is separated into two contributions: a flux of entropy due to the interactions of the system with its environment, which can be directed in or out of the system; and a source of entropy

due to interactions within the system. These interactions never create a sink of entropy (Prigogine, 1955). This separation is extremely useful in the present work because it allows us to concentrate on the estimation of the fluxes with the certainty that the unknown sources may only increase the entropy inside the system. Therefore, the expressions for the net source of entropy will not be discussed here but will be referred to, in a generic way, as "the irreversible generation of entropy." Its value per unit mass will be represented by σ. Hence, our task is reduced to finding appropriate expressions for the entropy fluxes.

Entropy fluxes may be due to mass fluxes carrying mass from one point to another as well as heat fluxes. Let's first consider the flux of entropy through the walls of a control volume due to mass transport. Such a flux can be written as

$$\mathbf{J}_s = \sum_j \rho_j s_j \mathbf{v}_j \tag{3.41}$$

Using equation (3.39), equation 3.41 can be written in terms of convective and diffusive transport as

$$\mathbf{J}_s = \rho\, s\, \mathbf{v}_d + \mathbf{D}_s \tag{3.42}$$

where

$$\mathbf{D}_s = \sum_j \rho_j s_j \mathbf{v}_{Dj} \tag{3.43}$$

is the diffusive flux of entropy. As mentioned before, associated with this flux there is a source of entropy whose unknown value we simply lumped into the irreversible source of entropy. Note that even though an expression for this source can be found in the book by de Groot and Mazur (1962), we still consider it as unknown because

it is very difficult to estimate from the data, for we do not have reliable information about the horizontal inhomogeneities in the system.

Heat transfers are due to conduction and/or radiation; recall that convection is implicitly taken into account in the mass fluxes.

Heat conduction is set up by the gradients in temperature through the system, which as a whole is not in thermodynamic equilibrium. Nevertheless, we can still assume that every small piece of the system is locally in thermodynamic equilibrium. Hence, the effect of heat conduction on the entropy of each piece of the system can be characterized by the amount of heat yielded or absorbed by this piece and by its absolute temperature, T. Therefore, we can write the change in entropy per unit time per unit volume due to conduction as

$$-\frac{1}{T}\boldsymbol{\nabla}\cdot\mathbf{J}_C \tag{3.44}$$

where $\mathbf{J}_C$ is the conductive heat flux. This expression can be considered as the conductive source of entropy for the system; however if a piece of matter is actually being cooled, this source becomes a sink of entropy. Therefore, this source does not behave in the expected way. Nevertheless, in this case the separation between flux and source of entropy can be formally established by rewriting the above expression as follows:

$$-\frac{1}{T}\boldsymbol{\nabla}\cdot\mathbf{J}_C = -\left[\boldsymbol{\nabla}\cdot\left(\frac{\mathbf{J}_C}{T}\right) + \frac{1}{T^2}\mathbf{J}_C\cdot\nabla T\right] \tag{3.45}$$

This suggests that the effect of heat conduction on the system's entropy can be regarded as composed of two parts: A flow of entropy through the boundary of the

system

$$\mathbf{J}_S = -\boldsymbol{\nabla}\cdot\left(\frac{\mathbf{J}_C}{T}\right) \tag{3.46}$$

and a generation of entropy inside the system

$$\mathcal{S} = -\frac{1}{T^2}\mathbf{J}_C \cdot \nabla T \tag{3.47}$$

The fact that this source is actually positive in the case of heat conduction comes from the property that the conductive heat flux, $\mathbf{J}_C$, is always directed against the gradient in temperature. It is noteworthy that this source of entropy is proportional to the gradient in temperature which is what set up the conduction process in the first place.

Radiative heating, on the other hand, is not necessarily set by the gradients in temperature of the system. Part of the radiation can travel through the system without interacting with it (for example visible radiation in the atmosphere) or may penetrate some distance before it interacts with the substance (Liou, 1980). Nevertheless, when the radiation field interacts with a part of the system, that part is heated or cooled, and its entropy is increased or decreased, respectively. Therefore, as in the case of conduction, the change in entropy per unit time per unit volume due to radiation can also be represented by

$$-\frac{1}{T}\boldsymbol{\nabla}\cdot\mathbf{J}_R \tag{3.48}$$

where $\mathbf{J}_R$ is the radiative heat flux. Contrary to the case of conduction in which the separation between flux and entropy generation is relatively simple, in the case of radiation such separation is only clear in the limit of diffusive radiation (Mihalas

and Mihalas, 1984). In any other radiative regime, this separation is not as simple, because the interaction between the matter and the radiation over the range of frequencies in the spectrum is quite complex. For instance, scattering processes in the atmosphere may lead to non-local thermodynamic situations. Even if the interactions are such that the atmosphere is in local thermodynamic equilibrium, it still could be far from the diffusive regime. These complexities force us to treat radiation as an external source of entropy whose value can be positive or negative, and is given by equation (3.48). Unfortunately, treating radiation as an external source has the disadvantage of requiring the value of this source at every point in the control volume. This is the reason that even though conduction and radiation are mathematically very similar, we do not treat conduction as an external source of the system.

Collecting all its elements, the budget equation for the entropy can be written as

$$\frac{d}{dt}\int_V \rho s \; dV = -\oint_S \left[\rho\, s\, \mathbf{v}_d + \mathbf{D}_s + \frac{1}{T}\mathbf{J}_C\right]\cdot \hat{\mathbf{n}} \; da - \int_V \frac{1}{T}\boldsymbol{\nabla}\cdot\mathbf{J}_R + \int_V \rho\sigma \; dV \qquad (3.49)$$

Using the fixed-control-volume technique (section 2.2), we arrive at the governing equation of entropy in flux form

$$\frac{\partial(\rho\, s)}{\partial t} + \boldsymbol{\nabla}\cdot[\rho\, s\, \mathbf{v} + \mathbf{D}_s + \frac{1}{T}\mathbf{J}_C] + \frac{1}{T}\boldsymbol{\nabla}\cdot\mathbf{J}_R = \rho\sigma \qquad (3.50)$$

Chapter 4

Explicit relationships

In the rest of this work, we will assume that the internal energy and the entropy per unit mass depend only on temperature, pressure and moisture. In this chapter, we present explicit expressions for these variables.

4.1 Internal energy

We define the internal energy per unit mass of the jth component in a multicomponent fluid as

$$u_j = c_{vj} T_j + u_{0j} \tag{4.1}$$

where c_{vj} is the heat capacity at constant volume, T_j is the absolute temperature, and u_{0j} is a constant of integration. This definition is quite general and can be used with gases as well as liquids and solids. Note, however, that for condensed matter there is almost no difference between heat capacities at constant pressure and constant volume in the atmospheric range of pressures.

The constants of integration in the internal energy definition are in general different for each of the components. Even so, the cloud condensate and liquid water The same is true for cloud ice and ice precipitation, which make up the solid phase. Furthermore, the integration constants for all water phases are not independent. This is because there are well defined energy gaps that separate the different phases of the water substance. Therefore, in order to obtain an explicit expression for the internal energies, we must find the relationships among the integration constants that appear in the internal energy definition. For such purpose, we use the enthalpy function, which is closely related to the internal energy. The reason for using the enthalpy is that, by definition of latent heat, the difference among the enthalpies of the water phases is equal to the latent heat release during the transformation from a less to a more ordered phase. That is, if h_v, h_l, and h_i are the vapor, liquid, and ice enthalpies per unit mass respectively, then

$$h_v - h_l = L_v(T) \tag{4.2}$$

$$h_v - h_i = L_s(T) \tag{4.3}$$

$$h_l - h_i = L_f(T) \tag{4.4}$$

where the temperature T is the absolute temperature at which the transition occurs and $L_v(T)$, $L_s(T)$, $L_f(T)$ are the latent heats of vaporization, sublimation, and fusion at temperature T, respectively.

The relationship between the internal energy and enthalpy per unit mass is

$$h_j = u_j + P_j \alpha_j \tag{4.5}$$

which for ideal gases can be written as

$$h_j = u_j + R_j T_j \tag{4.6}$$

where $R_j = R_g/\mathcal{M}_j$ is the gas constant of the jth gas; R_g is the universal gas constant and $\mathcal{M}_j$ is the molecular mass of that gas. As it stands, it seems that this definition of enthalpy cannot be applied to liquids and solids. However, we know that there is no difference between internal energy and enthalpy for the condensed cases for atmospheric conditions. So, equation (4.6) can be applied in such cases by setting the gas constant to zero. Using the definition of internal energy, equation (4.1), in equation (4.6) results in

$$h_j = c_{pj} T_j + u_{0j} \tag{4.7}$$

where the heat capacity at constant pressure is defined as

$$c_{pj} = c_{vj} + R_j \tag{4.8}$$

Again setting R_j to zero would result in the expected behavior for liquids and solids, where there is no difference between the two heat capacities.

It would be convenient to write the integration constants in terms of the temperature and pressure at some arbitrary reference point. Calling T_r and P_r the absolute temperature and pressure at the reference point, then the enthalpy at the reference point is given by

$$h_{rj} = c_{pj} T_r + u_{0j} \tag{4.9}$$

Therefore, the enthalpy can be written as

$$h_j = c_{pj}(T_j - T_r) + h_{rj} \tag{4.10}$$

Hence, equations (4.2-4.4) imply that at the reference point

$$h_{rl} = h_{rv} - L_v(T_r) \tag{4.11}$$

$$h_{ri} = h_{rv} - L_s(T_r) \tag{4.12}$$

$$h_{ri} = h_{rl} - L_f(T_r) \tag{4.13}$$

Unfortunately, only two of these equations are independent, which leaves one of the reference constants undefined. Nevertheless, these are the relationships that must be satisfied by the reference values of the water-substance enthalpies. Choosing the reference value of the enthalpy of ice as the arbitrary constant fixes the reference values for all water phases. On the other hand, the reference constant for dry air is independent of them. So, the enthalpy for the jth component in the fluid is given by equation (4.10) where the reference constants for water vapor and liquid water are given by

$$h_{rv} = L_s(T_r) + h_{ri} \tag{4.14}$$

$$h_{rl} = L_f(T_r) + h_{ri} \tag{4.15}$$

respectively; and the reference values of the enthalpy of ice, and dry air, at the reference point are arbitrary. These results can be translated into internal energies using equations (4.6) and (4.8), resulting in

$$u_d = c_{vd}(T_d - T_r) + u_{rd} \tag{4.16}$$

$$u_v = c_{vv}(T_v - T_r) + u_{rv} \tag{4.17}$$

$$u_l = c_l(T_l - T_r) + u_{rl} \tag{4.18}$$

$$u_i = c_i(T_i - T_r) + u_{rv} \tag{4.19}$$

where the reference constants are given by

$$u_{rd} = h_{rd} - R_d T_r \tag{4.20}$$

$$u_{rv} = h_{rv} - R_v T_r \tag{4.21}$$

$$u_{rl} = h_{rl} \tag{4.22}$$

$$u_{ri} = h_{ri} \tag{4.23}$$

The internal energy per unit mass of the fluid as a whole may be written as

$$\begin{aligned} u = {} & q_d[c_{vd}(T - T_r) + u_{rd}] \\ & + q_v[c_{vv}(T - T_r) + u_{rv}] \\ & + q_{cl}[c_l(T - T_r) + u_{rl}] \\ & + q_{ci}[c_i(T - T_r) + u_{ri}] \\ & + q_{pl}[c_l(T_l - T_r) + u_{rl}] \\ & + q_{pi}[c_i(T_i - T_r) + u_{ri}] \end{aligned} \tag{4.24}$$

where q_d, q_v, q_{cl}, q_{ci}, q_{pl}, q_{pi} are the partial concentrations of dry air, water vapor, cloud liquid, cloud ice, precipitating liquid water, and precipitating ice; we also have assumed a common temperature for all components except precipitating condensate.

4.2 Kinetic energy

The kinetic energy of the system per unit mass is defined as

$$K = \frac{1}{\rho} \sum_j \rho_j k_j \tag{4.25}$$

where k_j is the kinetic energy per unit mass for the jth component, which is defined as

$$k_j = \frac{1}{2}\mathbf{v_j} \cdot \mathbf{v_j} \tag{4.26}$$

where $\mathbf{v_j}$ is the average velocity of the jth component.

4.3 Potential energy

The potential energy of the system per unit mass is defined as

$$\phi = \frac{1}{\rho}\sum_j \rho_j \phi_j \tag{4.27}$$

where ϕ_j is the potential energy of the jth component. We assume that the only potential energy in the system is due to the gravitational field, so that, the potential energy of the jth component is given by

$$\phi_j = g\, z \tag{4.28}$$

where g is the acceleration of the gravity and z is the altitude above sea level. Therefore, the total potential energy per unit mass reduces to

$$\phi = g\, z \tag{4.29}$$

4.4 Bernoulli function

The Bernoulli function per unit mass for the system was defined in equation (3.35). Using the state equation for the ideal gases and the definition of total energy, the

Bernoulli function can be written as

$$
\begin{aligned}
b &= \frac{1}{\rho}\sum_j \rho_j b_j && (4.30)\\
&= \frac{1}{\rho}\sum_j \rho_j (e_j + P_j \alpha_j) && (4.31)\\
&= \frac{1}{\rho}\sum_j \rho_j (e_j + R_j T_j) && (4.32)\\
&= e + \sum_j q_j R_j T_j && (4.33)
\end{aligned}
$$

where q_j is the concentration of the jth component. Recalling that the gas constant for the condensed phases must be set to zero, and that the gaseous components share the same temperature, T, the expression for the Bernoulli function can be written as

$$b = e + T(q_d R_d + q_v R_v) \tag{4.34}$$

4.5 Entropy

We define the entropy per unit mass of the jth component in a multicomponent fluid as

$$s_j = c_{pj}\log(T_j) - R_j \log(P_j) + s_{0j} \tag{4.35}$$

where T_j and P_j are the absolute temperature and pressure of the component, c_{pj} is its heat capacity at constant pressure, R_j is the gas constant, and s_{0j} is a constant of integration. As with the definition of energy, for the entropy we set the gas constant to zero for all condensed phases. Also, the integration constants in the entropy definition of the water phases are not independent. In this case however, it is because the water phases must satisfy certain conditions when they are in thermodynamic equilibrium.

Let us first rewrite equation (4.35) in terms of the entropy value at some arbitrary reference point. Call T_r and P_r the temperature and pressure at the reference point. Then the entropy at the reference point is

$$s_{rj} = c_{pj} \log(T_r) - R_j \log(P_r) + s_{0j} \tag{4.36}$$

Substituting the integration constant back into the entropy definition results in

$$s_j = c_{pj} \log(T_j/T_r) - R_j \log(P_j/P_r) + s_{rj} \tag{4.37}$$

Now, in order to obtain the relationships among the reference constants in the expression for the entropy of the water phases, we need to analyze the equilibrium conditions between water phases. These conditions are that the temperature and pressure, as well as the chemical potentials, of the coexisting phases must be equal. The chemical potential of the jth component is defined as

$$\mu_j = h_j - s_j T_j \tag{4.38}$$

where h_j and s_j are the enthalpy and entropy per unit mass, respectively; and T_j is the absolute temperature.

Let us first analyze the equilibrium between water vapor and liquid water. For vapor to be in equilibrium with liquid water, the vapor must be saturated. Call $s_v^*(T, P_v^*)$ the entropy of water vapor at saturation, where P_v^* is the saturation vapor pressure; the entropy of liquid water at temperature T is $s_l(T)$. The enthalpies of water vapor and liquid water are $h_v(T)$ and $h_l(T)$, respectively. The condition for equilibrium at temperature T can be written as

$$h_v(T) - T\, s_v^*(T, P_v^*) = h_l(T) - T\, s_l(T) \tag{4.39}$$

Using the definition of latent heat of vaporization, equation(4.2), we obtain

$$s_l(T) = s_v^*(T, P_v^*) - \frac{L_v(T)}{T} \tag{4.40}$$

Since

$$s_v^*(T, P_v^*) = c_{pv} \log(T/T_r) - R_v \log(P_v^*/P_r) + s_{rv} \tag{4.41}$$

and

$$s_l = c_l \log(T/T_r) + s_{rl} \tag{4.42}$$

evaluating equation (4.40) at the reference point results in

$$s_{rl} = s_{rv} - \frac{L_v(T_r)}{T_r} \tag{4.43}$$

which is the relation between the liquid water and water vapor reference entropies.

Similar procedures lead to the relationships between the ice and water vapor

$$s_{ri} = s_{rv} - \frac{L_s(T_r)}{T_r} \tag{4.44}$$

and between liquid water and ice

$$s_{ri} = s_{rl} - \frac{L_f(T_r)}{T_r} \tag{4.45}$$

where $L_s(T_r)$ and $L_f(T_r)$ are the latent heats of sublimation and fusion, respectively. Again, only two of these relationships are independent leaving one of the reference constants undetermined.

A general relationship between the liquid water and water vapor entropies can be obtained by noting that

$$s_v^*(T, P_v^*) = s_v(T, P) + R_v \log(H_l) \tag{4.46}$$

where H_l is the relative humidity with respect to liquid water,

$$H_l = \frac{P_v}{P_v^*} \tag{4.47}$$

With equation (4.46) in (4.40), we have

$$s_l(T) = s_v(T, P) + R_v \log(H_l) - \frac{L_v(T)}{T} \tag{4.48}$$

as the general relationship between the liquid water and water vapor entropies.

A similar relationship between ice and water vapor entropies can also be obtained, namely,

$$s_i(T) = s_v(T/T_r) + R_v \log(H_s) - \frac{L_s(T)}{T} \tag{4.49}$$

where $L_s(T)$ is now the sublimation latent heat and H_s is the relative humidity with respect to ice.

The entropy per unit mass of the fluid as a whole may be written as

$$\begin{aligned} s \;=\; & q_d(c_{pd}\log(T/T_r) - R_d\log(P_d/P_r) + s_{rd}) \\ & + q_v(c_{pv}\log(T/T_r) - R_v\log(P_v/P_r) + s_{rv}) \\ & + q_{cl}(c_l\log(T/T_r) + s_{rl}) \\ & + q_{ci}(c_i\log(T/T_r) + s_{ri}) \\ & + q_{pl}(c_l\log(T_l/T_r) + s_{rl}) \\ & + q_{pi}(c_i\log(T_i/T_r) + s_{ri}) \end{aligned} \tag{4.50}$$

where q_d, q_v, q_{cl}, q_{ci}, q_{pl}, q_{pi} are the partial concentrations of dry air, water vapor, cloud liquid, cloud ice, precipitating liquid water, and precipitating ice. We have assumed a common temperature for all components, except for precipitating condensate terms.

This expression has two undefined constants: the reference values of the entropy of dry air and water vapor.

In order to compare this expression to others found in the literature, we reduce it to the case where there is only dry air, water vapor and cloud liquid water in the atmosphere. All components are assumed to have the same temperature. Thus, the entropy reduces to

$$s = q_d s_d + q_v s_v + q_{cl} s_{cl} \tag{4.51}$$

With the help of equation (4.48), this last equation can be written as

$$s = q_d s_d + q_v \left(s_{cl} - R_v \log(H_l) + \frac{L_v(T)}{T} \right) + q_{cl} s_{cl} \tag{4.52}$$

Regrouping terms, we have

$$s = q_d s_d + (q_v + q_{cl}) s_{cl} + q_v \left(-R_v \log(H_l) + \frac{L_v(T)}{T} \right) \tag{4.53}$$

Now using the definitions for dry air and liquid water entropies plus some algebra, we have

$$\begin{aligned} s = q_d \left[(c_{pd} + r_t\, c_l) \log(T/T_r) \right. \quad - \quad & R_d \, \log(P_d/P_r) - r_v \, R_v \, \log(H_l) + \frac{r_v L_v(T)}{T} \\ & \left. + (s_{rd} + r_t s_{rv}) \right] \end{aligned} \tag{4.54}$$

where we have defined $r_t = (q_v + q_{cl})/q_d$ as the total water mixing ratio and $r_v = q_v/q_d$ as the water vapor mixing ratio.

Many authors argue that the entropy, which for this particular system is called "moist entropy", is a conserved variable. Thus, they define moist entropy as

$$s = (c_{pd} + r_v\, c_l) \log(T/T_r) - R_d \, \log(P_d/P_r) - r_v \, R_v \, \log(H_l) + \frac{r_v L_v(T)}{T} \tag{4.55}$$

which is correct if the total mass fractions of dry air and water vapor can be regarded as constants. This may be appropriate for the analysis of closed parcels. Otherwise, the last term in equation (4.54), $(s_{rd} + r_t s_{rv})$, and also the factor q_d, turn out to be important. A simple example is the retrieving of the atmosphere's entropy profile from a sounding. In such a case, the total mixing ratio of water is changing all the way from the surface to the tropopause. Note that the form of such profiles depends on the reference values of the dry air and water vapor entropies.

Since usually equation (4.55) represents all liquid water, it could misrepresent the entropy of precipitation liquid water, which may not be at the same temperature as the cloud liquid water. We believe that equation (4.50), which by the way includes ice processes, is an improvement over equation (4.55) in representing the entropy in the atmosphere.

Chapter 5

Tendency equations

In this chapter, we use the budget analysis technique to estimate the tendencies — that is, the time rate of change — of the average values of total water, total energy, and entropy. This technique consists in the integration of the differential governing equations in a particular control volume. We do this integration over a cylinder that extends from the surface to an upper boundary whose altitude is high enough to hold all possible convection beneath it. Its lateral boundary is also loosely defined, but it has to be large enough to enclose convection, see figure (5.1).

Calling any of our density variables ψ, then the time rate of change of the average value of ψ over the control cylinder is defined as

$$\frac{d\overline{\psi}}{dt} = \frac{d}{dt}\left[\frac{1}{A\,H}\int_{\mathsf{V}} \psi \;\, dV\right] \tag{5.1}$$

where A is the horizontal area of the control cylinder, H is its height, and V is its volume.

In order to make this integration possible, some approximations are in order: The

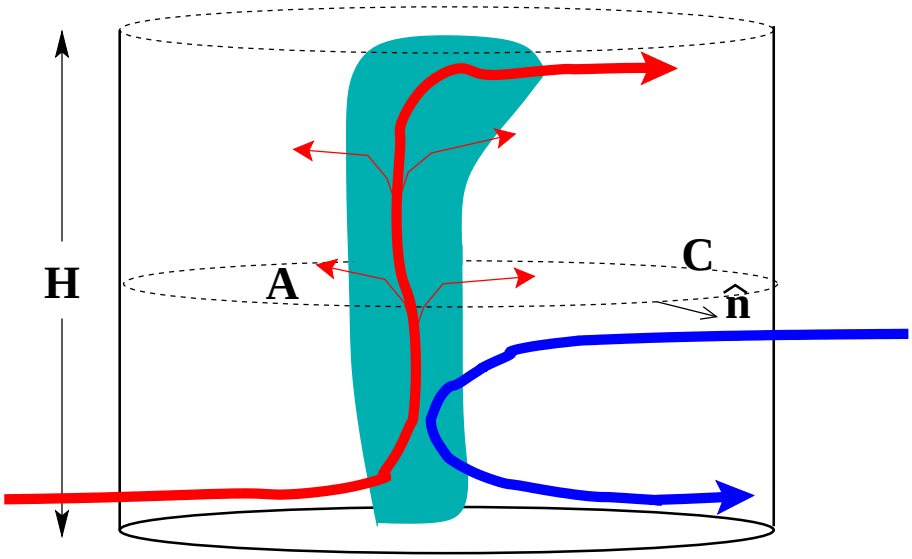

Figure 5.1: Sketch of a typical control volume used in this work.

horizontal velocity of cloud condensate will be regarded as equal to the horizontal mean velocity of the fluid; this is a standard assumption made in radar meteorology (Doviak, 1984). Note that the vertical velocity of the condensate can still be very different from the mean flow velocity, especially at the lower boundary. At the upper boundary we assume that no flux of matter can exist: basically this is the definition of the upper boundary. Regarding heat fluxes, we assume that all radiative and conductive heat fluxes are uniform at each of the three boundaries of the cylinder; we assume no heat conduction through the upper and lateral boundaries as well as no horizontal radiative fluxes. We also assume uniform temperatures at the lower and upper boundaries.

5.1 Water substance

Using basically the fixed-control-volume technique (2.2) in reverse order, we can integrate the total water governing equation in the control cylinder as follows:

$$\frac{d}{dt}\int_{\mathsf{V}} \rho_w \ dV = -\oint_{\mathsf{A}} (\rho_w \mathbf{v}_d + \mathbf{D}_w) \cdot \hat{\mathbf{n}} \ da \tag{5.2}$$

Dividing the surface integral into the three parts that make up the cylinder's area (bottom, top, and lateral boundaries) and applying the assumptions of no matter-flux whatsoever through the upper boundary, no diffusive flux of matter through the lateral boundary, and no mean flow of dry air through the lower boundary, results in

$$\frac{d}{dt}\int_{\mathsf{V}} \rho_w \ dV = -\left\{\int_{\mathsf{lat}} \rho_w \mathbf{v}_d \cdot \hat{\mathbf{n}}_l \ da + \int_{\mathsf{bott}} \mathbf{D}_w \cdot \hat{\mathbf{n}}_s \ da\right\} \tag{5.3}$$

where $\hat{\mathbf{n}}_l$ and $\hat{\mathbf{n}}_s$ are the unit vectors pointing outward from the volume at the lateral and bottom surfaces, respectively. Since at the bottom surface the only diffusive fluxes are due to evaporation and precipitation (ice and/or liquid), we have that

$$\mathbf{D}_w \cdot \hat{\mathbf{n}}_s = (\rho_v \mathbf{v}_{Dv} + \rho_{pl} \mathbf{v}_{Dpl} + \rho_{pi} \mathbf{v}_{Dpi}) \cdot \hat{\mathbf{n}}_s \tag{5.4}$$

where the subindexes v, pl, and pi refer to vapor, liquid precipitation, and ice precipitation. Since the mean value of the dry air vertical velocity is zero at the surface, the diffusive flux of vapor at the surface is, by definition, just the evaporation rate, $\mathcal{E}$, and the total diffusive flux of precipitation is just the precipitation rate of liquid water, $\mathcal{P}_l$, plus the precipitation rate of ice, $\mathcal{P}_i$. Hence, we have

$$\mathbf{D}_w \cdot \hat{\mathbf{n}}_s = -\mathcal{E} + \mathcal{P}_l + \mathcal{P}_i \tag{5.5}$$

The minus sign in front of the evaporation rate is due to fact that evaporation is defined as going into the atmosphere and the normal to the surface is pointing out

of the atmosphere. With this result and the definition of the average value of water substance, equation (5.3) can be written as

$$\frac{d\overline{\rho_w}}{dt} = \frac{-1}{A\,H}\left\{\int_{\mathsf{lat}} \rho_w \mathbf{v}_d \cdot \hat{\mathbf{n}}_l \;\; da + \int_{\mathsf{bott}} (-\mathcal{E} + \mathcal{P}_l + \mathcal{P}_i) \;\; da\right\} \tag{5.6}$$

5.2 Total energy tendency

In a very similar way, we can write a tendency equation for the average total energy inside the control cylinder:

$$\begin{aligned}\frac{d\overline{\rho e}}{dt} \;=\; & \frac{-1}{A\,H}\left\{\int_{\mathsf{lat}} (\rho\, b\, \mathbf{v}_d + \mathbf{J}_W - \overleftrightarrow{\nu} \cdot \mathbf{v}) \cdot \hat{\mathbf{n}}_l \;\; da \right. \\ & + \int_{\mathsf{top}} (\mathbf{J}_{R,t} + \mathbf{J}_W - \overleftrightarrow{\nu} \cdot \mathbf{v}) \cdot \hat{\mathbf{k}} \;\; da \\ & \left. + \int_{\mathsf{bott}} [\mathbf{J}_{R,b} + \mathbf{J}_C + \mathbf{D}_b - (\overleftrightarrow{\nu} \cdot \mathbf{v})] \cdot (-\hat{\mathbf{k}}) \;\; da\right\}\end{aligned} \tag{5.7}$$

where $\hat{\mathbf{k}}$ is the unit vector in the z direction. Other symbols are defined in section (3.7).

Call

$$\mathcal{L} = \frac{1}{A\,H} \oint_{\mathsf{A}} \overleftrightarrow{\nu} \cdot \mathbf{v} \cdot \hat{\mathbf{n}} \;\; da \tag{5.8}$$

the total energy dissipated by frictional stress at the surface of the control cylinder, and

$$\mathcal{W} = \frac{-1}{A\,H} \oint_{\mathsf{A}} \mathbf{J}_W \cdot \hat{\mathbf{n}} \;\; da \tag{5.9}$$

the total energy flushed out of the control cylinder by wave action. Then equation (5.7) can be written as

$$\begin{aligned}\frac{d\overline{\rho e}}{dt} \;=\; & \frac{-1}{A * H}\left\{\int_{\mathsf{lat}} \rho\, b\, \mathbf{v}_d \cdot \hat{\mathbf{n}}_l \;\; da + \int_{\mathsf{top}} \mathbf{J}_{R,t} \cdot \hat{\mathbf{k}} \;\; da \right. \\ & \left. + \int_{\mathsf{bott}} (\mathbf{J}_{R,s} + \mathbf{J}_C + \mathbf{D}_b) \cdot (-\hat{\mathbf{k}}) \;\; da\right\} + \mathcal{L} + \mathcal{W}\end{aligned} \tag{5.10}$$

Since the diffusive flux of the Bernoulli function at the surface can be written as

$$\mathbf{D}_b \cdot (-\hat{\mathbf{k}}) = (\rho_v\, b_v\, \mathbf{v}_{Dv} + \rho_{pl}\, b_{pl}\, \mathbf{v}_{Dpl} + \rho_{pi}\, b_{pi}\, \mathbf{v}_{Dpi}) \cdot (-\hat{\mathbf{k}}) \tag{5.11}$$

$$= -\mathcal{E}\, b_{v,b} + \mathcal{P}_l\, b_{pl,b} + \mathcal{P}_i\, b_{pi,b} \tag{5.12}$$

where $\mathcal{E}$, $\mathcal{P}_l$, and $\mathcal{P}_i$ are the evaporation, liquid water, and ice precipitation rates, respectively, the tendency equation (5.10) can be written as

$$\begin{aligned}\frac{d\overline{\rho e}}{dt} = \frac{-1}{A\,H}\Bigg\{ & \int_{\mathsf{lat}} \rho\, b\, \mathbf{v}_d \cdot \hat{\mathbf{n}}_l \; da + \int_{\mathsf{top}} \mathbf{J}_{R,t} \cdot \hat{\mathbf{k}} \; da \\ & + \int_{\mathsf{bott}} \left[(\mathbf{J}_{R,s} + \mathbf{J}_C) \cdot (-\hat{\mathbf{k}}) - \mathcal{E}\, b_{v,b} + \mathcal{P}_l\, b_{pl,b} + \mathcal{P}_i\, b_{pi,b} \right] \; da \Bigg\} \\ & + \mathcal{L} + \mathcal{W}\end{aligned} \tag{5.13}$$

where $b_{v,b}$, $b_{pl,b}$, $b_{pi,b}$ are the Bernoulli functions of vapor, liquid precipitation and ice precipitation at the bottom surface, respectively. Note that the Bernoulli functions for the condensed phases are the same as the total energy of those phases. This is so because the internal energy and the enthalpy are the same in those cases.

5.3 Entropy tendency

Integration of the entropy governing equation over the control cylinder leads to the following tendency equation for the average entropy:

$$\begin{aligned}\frac{d\overline{\rho\, s}}{dt} = \frac{-1}{A\,H}\Bigg\{ & \int_{\mathsf{lat}} \rho\, s\, \mathbf{v}_d \cdot \hat{\mathbf{n}}_l \; da \\ & + \int_{\mathsf{bott}} \left[\frac{\mathbf{J}_C}{T_s} \cdot (-\hat{\mathbf{k}}) - \mathcal{E}\, s_{v,b} + \mathcal{P}_l\, s_{pl,b} + \mathcal{P}_i\, s_{pi,b} \right] \; da \Bigg\} + \mathcal{R} + \mathcal{G}\end{aligned} \tag{5.14}$$

where $s_{v,b}$, $s_{pl,b}$, $s_{pi,b}$ are the entropy of vapor, liquid precipitation and ice precipitation at the bottom surface, respectively;

$$\mathcal{R} = \frac{-1}{A\,H} \int_{\mathsf{V}} \frac{1}{T} \boldsymbol{\nabla} \cdot \mathbf{J}_R \; dV \tag{5.15}$$

is the average change in entropy due to radiation; and

$$\mathcal{G} = \frac{1}{A\,H} \int_{\mathsf{V}} \rho \sigma \; dV \tag{5.16}$$

is the average irreversible generation of entropy inside the control cylinder; the temperature distribution at the bottom surface is T_s. Other quantities are defined in section (3.8).

5.4 Getting rid of precipitation

In order to make estimates of the tendencies presented in the previous sections, we need among other things the distribution of precipitation at the surface. Aside from the estimation of the sources $\mathcal{L}$, $\mathcal{W}$, and $\mathcal{G}$, precipitation is the most difficult variable to estimate from field data. It is so uncertain that most attempts to estimate it have error bars somewhere between 50 and 150 percent. This is in fact the basic limitation that precludes the use of the total water tendency equation by itself to examine the drying/moistening effects of convective clouds on their environment.

Here, we present an alternative method that eliminates the necessity of knowing the precipitation distribution so long as there is no ice precipitation reaching the surface. This is a reasonable assumption in the deep tropics. Other required assumptions are that temperature and pressure are constant throughout the bottom

surface and that the kinetic energy is much smaller than the internal energy at the surface. Given these assumptions, then the total energy as well as the entropy can be considered constant at the bottom surface of the control cylinder.

Multiplying the tendency equation for total water (5.6) by $b_{pl,b}$ and subtracting the result from the tendency equation of total energy (5.13), we obtain

$$\begin{aligned}\frac{d(\overline{\rho e} - \overline{\rho_w b_{pl,b}})}{dt} &= \frac{-1}{A\,H}\left\{\int_{\mathsf{lat}} (\rho\, b\, \mathbf{v}_d - \rho_w b_{pl,b}\mathbf{v}_d)\cdot\hat{\mathbf{n}}_l \;\, da + \int_{\mathsf{top}} \mathbf{J}_{R,t}\cdot\hat{\mathbf{k}} \;\, da \right. \\ &\quad \left. + \int_{\mathsf{bott}} \left[(\mathbf{J}_{R,s} + \mathbf{J}_C)\cdot(-\hat{\mathbf{k}}) - \mathcal{E}(b_{v,b} - b_{pl,b})\right] \;\, da\right\} \\ &\quad + \mathcal{L} + \mathcal{W} \end{aligned} \tag{5.17}$$

which can be written as

$$\begin{aligned}\frac{d\overline{\rho(e - q_w\, e_{pl,b})}}{dt} &= \frac{-1}{A\,H}\left\{\int_{\mathsf{lat}} \rho\,(b - q_w b_{pl,b})\,\mathbf{v}_d\cdot\hat{\mathbf{n}}_l \;\, da + \int_{\mathsf{top}} \mathbf{J}_{R,t}\cdot\hat{\mathbf{k}} \;\, da \right. \\ &\quad \left. + \int_{\mathsf{bott}} \left[(\mathbf{J}_{R,s} + \mathbf{J}_C)\cdot(-\hat{\mathbf{k}}) - \mathcal{E}(b_{v,b} - b_{pl,b})\right] \;\, da\right\} \\ &\quad + \mathcal{L} + \mathcal{W} \end{aligned} \tag{5.18}$$

where q_w is the mass fraction of total water, and we have used the fact that the total energy and Bernoulli function are the same for condensed matter, so $b_{pl,b} = e_{pl,b}$. Defining the new variables

$$\varepsilon = e - q_w\, e_{pl,b} \tag{5.19}$$

$$\Upsilon = b - q_w b_{pl,b} \tag{5.20}$$

results in a new governing equation.

$$\begin{aligned}\frac{d\overline{\rho\varepsilon}}{dt} &= \frac{-1}{A\,H}\left\{\int_{\mathsf{lat}} \rho\,\Upsilon\,\mathbf{v}_d\cdot\hat{\mathbf{n}}_l \;\, da + \int_{\mathsf{top}} \mathbf{J}_{R,t}\cdot\hat{\mathbf{k}} \;\, da \right. \\ &\quad \left. - \int_{\mathsf{bott}} \left[(\mathbf{J}_{R,s} + \mathbf{J}_C)\cdot\hat{\mathbf{k}} + \mathcal{E}(b_{v,b} - b_{pl,b})\right] \;\, da\right\} + \mathcal{L} + \mathcal{W} \end{aligned} \tag{5.21}$$

Two things are notable about this governing equation: 1) It does not depend on precipitation. 2) Its source term is the same as that for the total energy.

Similarly, multiplying the tendency equation for total water by $s_{pl,b}$, and subtracting the result from the tendency equation of entropy (5.14), leads to

$$\begin{aligned} \frac{d\overline{\rho\,\varsigma}}{dt} &= \frac{-1}{A\,H}\left\{\int_{\mathsf{lat}} \rho\,\varsigma\,\mathbf{v}_d\cdot\hat{\mathbf{n}}_l\;da \right. \\ &\qquad \left. -\int_{\mathsf{bott}}\left[\frac{\mathbf{J}_C}{T_s}\cdot\hat{\mathbf{k}}+\mathcal{E}(s_{v,b}-s_{pl,b})\right]\;da\right\}+\mathcal{R}+\mathcal{G} \end{aligned} \tag{5.22}$$

where

$$\varsigma = s - q_w s_{pl,b} \tag{5.23}$$

The governing equation for this new variable does not contain precipitation and its source is the same as that for the entropy.

Chapter 6

Moistening and drying tendency equations

We have derived tendency equations for the average energy and entropy of the atmosphere. We have shown that in the case of no ice precipitation reaching the surface, those equations can be modified in such a way that they do not depend on precipitation. As long as the gradients in temperature are small and we are able to estimate all fluxes involved plus the corresponding source terms, each of these modified tendency equations can be used to study the moistening or drying of the environment by convective clouds. However, it turns out that the estimation of the sources of energy and entropy are probably more difficult to estimate than precipitation rates. Nevertheless, it is the purpose of this chapter to show how the modified tendency equations can be used to distinguish moistening from drying environments without the necessity of knowing the energy or entropy sources.

Let us begin by representing all the terms that can be estimated from field data

on the left hand side of (5.21) and (5.22) by E_{data} and S_{data}, respectively. That is,

$$E_{data} = \frac{-1}{A\,H}\left\{\int_{\mathsf{lat}} \rho\,\Upsilon\,\mathbf{v}_d\cdot\hat{\mathbf{n}}_l\;da + \int_{\mathsf{top}} \mathbf{J}_{R,t}\cdot\hat{\mathbf{k}}\;da - \int_{\mathsf{bott}}\left[(\mathbf{J}_{R,s}+\mathbf{J}_C)\cdot\hat{\mathbf{k}} + \mathcal{E}(b_{v,b}-b_{pl,b})\right]\;da\right\} \tag{6.1}$$

$$S_{data} = \frac{-1}{A\,H}\left\{\int_{\mathsf{lat}} \rho\,\varsigma\,\mathbf{v}_d\cdot\hat{\mathbf{n}}_l\;da - \int_{\mathsf{bott}}\left[\frac{\mathbf{J}_C}{T_s}\cdot\hat{\mathbf{k}} + \mathcal{E}(s_{v,b}-s_{pl,b})\right]\;da + \int_{\mathsf{V}}\frac{1}{T}\boldsymbol{\nabla}\cdot\mathbf{J}_R\;dV\right\} \tag{6.2}$$

Therefore, equations (5.21) and (5.22) can be rewritten as follows

$$\frac{d\overline{\rho\varepsilon}}{dt} = E_{data} + \mathcal{L} + \mathcal{W} \tag{6.3}$$

$$\frac{d\overline{\rho\varsigma}}{dt} = S_{data} + \mathcal{G} \tag{6.4}$$

We argue that the source of entropy, $\mathcal{G}$, is always positive, because it represents the internal generation of entropy for a system that is not in equilibrium. On the other hand, we argue that the source of energy, $\mathcal{L}$, must be negative, because it represents the viscous forces acting on the boundaries of the control cylinder. The wave energy source, $\mathcal{W}$, is also negative under the assumption that all waves are created by convective activity inside the control cylinder. That is, the dynamical response of a less active environment consumes energy from the convection.

Given these assumptions, a situation where E_{data} is negative implies that $d\overline{\rho\varepsilon}/dt$ is also negative. On the contrary, positive values of E_{data} leave the sign of $d\overline{\rho\varepsilon}/dt$ undetermined. Thus, the modified energy equation tells us whether drying is occurring in the control cylinder, but it cannot give a conclusive answer about moistening situations. Positive values of S_{data}, on the other hand, imply that $d\overline{\rho\varsigma}/dt$ is also positive, while for negative values of S_{data} the modified entropy equation is not conclusive.

As a result of this analysis, the modified energy equation can be used to identify situations when drying is occurring. We call this equation "the drying tendency equation". The modified entropy equation, on the other hand, can be used to identify moistening situations. We call it "the moistening tendency equation".

From the point of view of the data available to make the estimations of the different terms in the modified equations, we know that: radiation fluxes are relatively simple to estimate, as well as evaporation and conductive heat fluxes which can be parameterized in a simple fashion using surface data. On the other hand, good estimations for fluxes through the lateral boundary due to different kinds of convective activity are much more difficult to obtain. This is because typically those estimations come from sounding arrays which only are able to measure the net effect of the environmental plus all the convective activity inside the array. Good estimates of lateral fluxes are required to solve the budget equations, and therefore, they are crucial in understanding the nature of moisture interchange between clouds and their environments. Even though we need all terms except the sources to reach a definite conclusion about the influence of a convective system over its environment, understanding the moisture tendency due to individual terms is also valuable.

Given their importance, and the kind of data available to us, we will focus on the lateral contributions to the modified budget equations.

Part II

Data Analysis &

Results

Chapter 7

Data Sources

In this part, we use the theory developed in part I and the radar analysis techniques of section B.4 to address the scientific questions posed in the introduction:

- Is there a correlation between cloud-top and environmental moisture on a case-by-case basis ?
- What is the nature of the moisture interchange between clouds and environment?

Our data analysis is restricted to a limited region over the western Pacific and involves many assumptions. Therefore, it only offers an approximate answer for these questions. Far from being general, the results could be regarded only as an example of application of the theory developed in part I. Nevertheless, they strongly suggest the role of different convective regimes on the atmospheric moisture budget.

For our analysis, we use several data sets collected during the field phase of TOGA-COARE (Webster and Lukas, 1992). This phase of the experiment took place from 1

November 1992 to 28 February 1993, over the western Pacific warm pool. This region is characterized by sea surface temperatures that exceed 28°, and extends approximately from 10°S to 10°N and from 140°E to 170°E. (See figure 7.1.) During these four months, many kinds of measurements were made from a variety of platforms. Of primary importance to us are the Doppler velocities measured by the X-band Doppler radars mounted on the tails of the two National Oceanic and Atmospheric Administration(NOAA) WP-3D aircraft. Also crucial to this work are the flight level in-situ data collected by the WP-3D aircraft. These data are scientific and navigation fields sampled at a 1 Hz rate along the flight track. We use the wind speed and navigation parameters from these fields during our Doppler synthesis. The thermodynamic fields collected during flights are not used; instead, the thermodynamic structure for the whole depth of the troposphere is obtained from balloon soundings launched from the R/V *Moana Wave* , R/V *Xiangyanghong 5* , R/V *Shiyan 3* , and Kapingamarangi station. We also use images of the infrared brightness temperatures from the GMS-4 Japanese satellite (Flament and Bernstein, 1993). These images are used primarily for providing a context for the analysis, and in particular they help in the selection of the sounding used in the calculations of each case study. We focus our analysis on ten case-studies observed during TOGA-COARE. Table 7.1 lists the selected data for these cases. In chapters 8 and 9, we discuss how the raw data from soundings and radars were prepared before we use them to address the posed questions, which are tackled in chapters 10, 11.

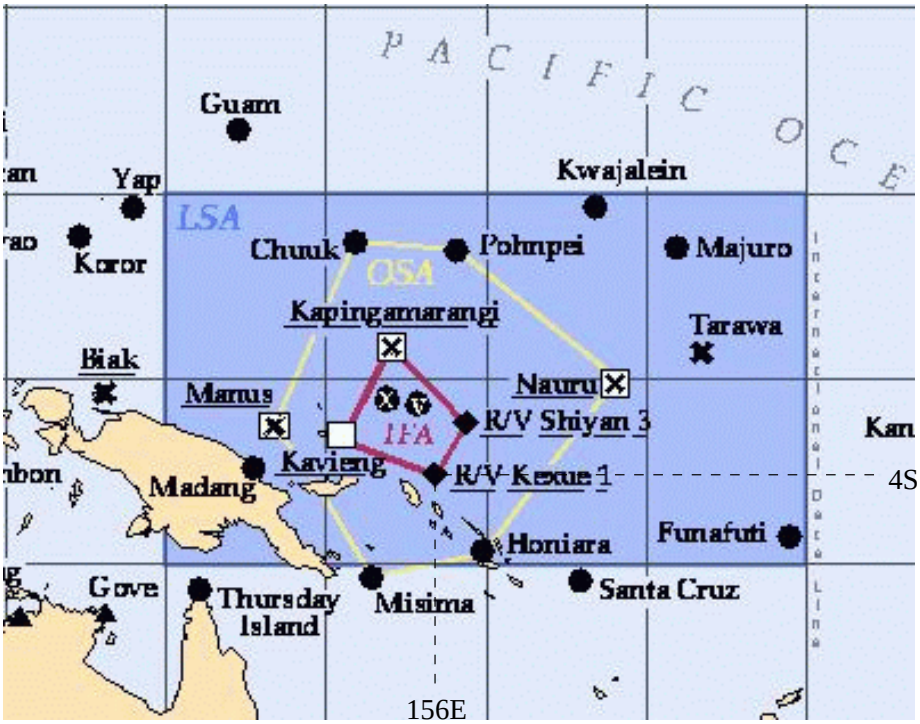

Figure 7.1: Area studied during the field phase of TOGA-COARE, including the primary sounding sites. The intensive flux array (IFA) is formed by the vessels *Shiyan 3* and *Kexue*, and the islands of Kapingamarangi and Kavieng. Most of our sounding data come from this array. However, we also use soundings from the R/V *Moana Wave* and *Xiangyanghong 5* (not pictured) which were working also close to the IFA. All aircraft missions were flown inside the large scale array (LSA) – most of them very close to the IFA. WP-3 aircraft flew from Honiara toward their target region and back to Honiara. Figure adapted from the station map in TOGA-COARE project description. Available: http://www.joss.ucar.edu/data/toga_coare

Table 7.1 Data Sources

Mission	Platforms		AD	Data Selected Times		System Velocity	
	BS	ACR		LT	RTI	V_x	V_y
			(km)	(UTC)	(UTC)	($m\,s^{-1}$)	($m\,s^{-1}$)
921126	SH	W43	250	-0115	0338–0636	0.00	-3.00
921128	MW	W42	20	0441	0352–0445	-2.82	2.82
921212	KP	BWP	665	1706	1747–1826	2.12	-2.12
921213	KP	W43	435	1656	1826–2041	0.00	10.00
921215	XY	W42	160	1714	1713–1837	-4.90	-4.90
930111	MW	W42	75	2255	2256–2520	2.80	2.80
930116	SH	W42	200	2302	2311–2430	9.00	0.00
930118	SH	W43	350	2300	0211–0355	3.50	-3.50
930201	MW	W42	70	2257	2251–2351	-7.70	7.70
930209	XY	BWP	505	1646	1632–1841	-4.20	-4.20

Table 7.1: Information about the data sources used in this work. The following are the meanings of the labels. BS = Balloon sounding: SH = R/V *Shiyan 3* ; MW = R/V *Moana Wave* ; XY = R/V *Xiangyanghong 5* ; KP = Kapingamarangi. ACR = radar data: BWP means both WP-3D aircraft. AD = Average distance between soundings and aircraft target area. LT = Balloon launching time; RTI = selected time intervals for Doppler analysis in each mission. The Cartesian components of the system velocity were calculated from the values reported in Kingsmill and Houze (1999) – they are positive in the east (V_x) and north (V_y) directions.

Chapter 8

Soundings

For each case study, we choose a single sounding launched close, both in space and time, to the studied region. In every case, special effort was made to avoid soundings that might already have been affected by the cloud system, as judged by the soundings' position with respect to the cloud system. This was made by visual inspection of plots where the sounding location, aircraft's target region, and infrared temperatures, were laid together. Figure 8.1, which shows the case of January 16, is an example of this kind of plot. For this case, the system was moving toward the east at 9 $\mathrm{m\,s^{-1}}$ and the sounding location appears to be ahead of the system. Table 7.1 lists the selected soundings for each case study.

The primary sounding data used in our analysis are: total pressure (P_t), environmental temperature (T_e), dew point temperature (T_d), altitude (z), and horizontal wind speed (v_h). These measurements are used to estimate profiles of three key functions in our work: moist energy (ε), moist entropy (ς), and the Bernoulli function (Υ), plus their saturated values. These functions are defined by equations (5.19),

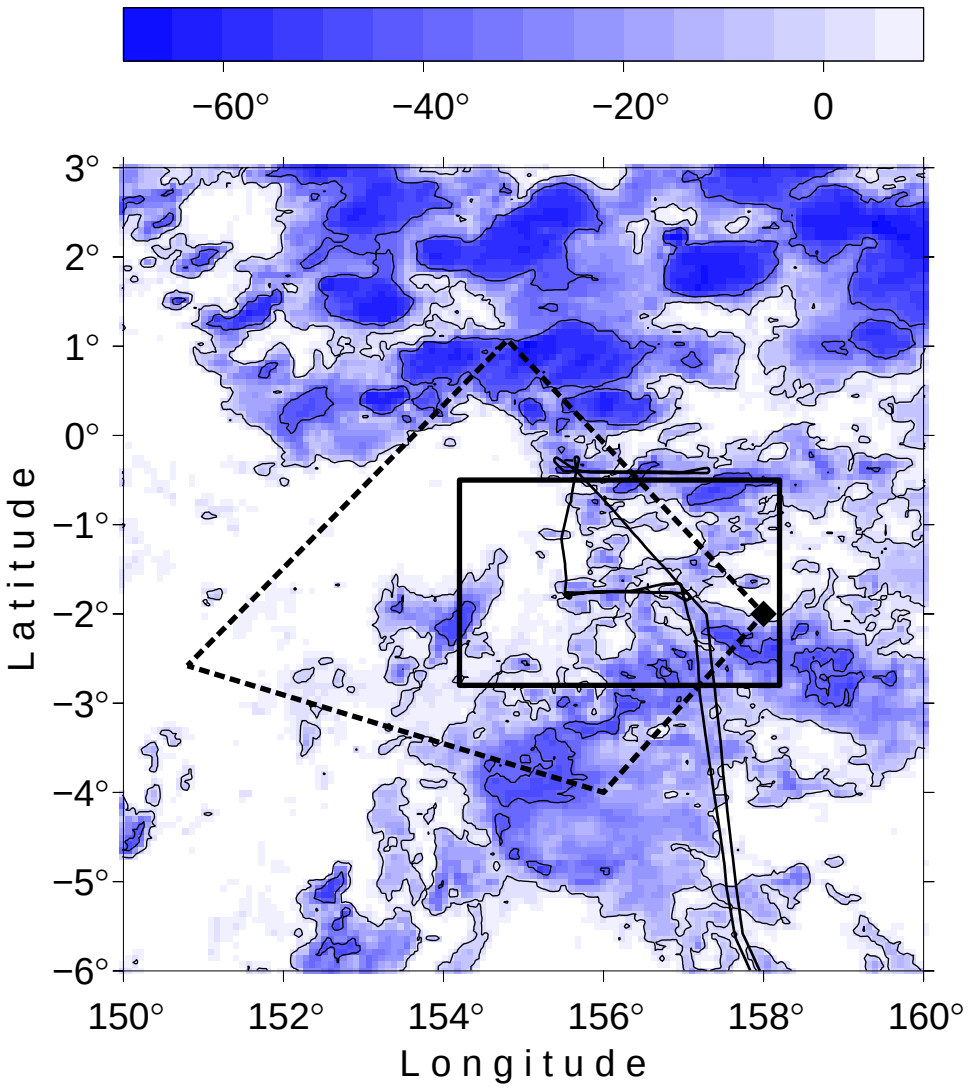

Figure 8.1: Relative location between sounding and the aircraft target area for the case of January 16, 1993. The system was moving toward the east. The background shading is the infrared brightness temperature from the GMS-4 Japanese satellite taken at 2315 UTC. Infrared temperatures are in degrees Celsius. The dashed polygon represents the intensive flux array(IFA), while the target area is enclosed by the rectangle. The aircraft path (thin-solid line) reached the target area approximately at 2300 UTC. The sounding was launched at 2302 UTC by the *Shiyan 3* (solid diamond at the most right corner of the IFA and ahead of the system).

(5.23), and (5.20), respectively.

In addition to these key functions, the soundings are used to estimate surface parameters and the temperature at the upper surface of the control cylinder (chapter 5). Some of the constants required in our calculations are listed in table 8.1.

The estimation of our key variables and surface parameters requires an estimation of the concentrations of the different components and their saturated values. Since balloon soundings do not contain any information about precipitation, we assume that they were made in clear air. Therefore, the only components of the atmosphere seen by the sounding instruments are dry air and water vapor. In this case, the total water concentration (q_w) is reduced to the water vapor concentration, and the concentration of dry air (q_d) and water vapor concentration (q_v) are related by the equation $q_d + q_v = 1$. Therefore, we only need the water vapor concentration and its saturated value q_v^*. These two quantities are obtained from the sounding primary data using the equations

$$q = \frac{\epsilon P_v^*(T_d)}{P_t + (\epsilon - 1) P_v^*(T_d)} \tag{8.1}$$

$$q^* = \frac{\epsilon P_v^*(T_e)}{P_t + (\epsilon - 1) P_v^*(T_e)} \tag{8.2}$$

where $\epsilon = R_d/R_v$ is the ratio of the gas constants of dry air to water vapor; and $P_v^*(T)$ is the saturated vapor pressure at temperature T. It should be pointed out that saturation above freezing level is taken with respect to ice, while below this level, it is taken with respect to liquid water. Thus, we have chosen to approximate the saturation vapor pressure by using Bolton's formula below the freezing level, and by

Table 8.1 Constants

Symbol	value	units	Description
T_s	30	C	Sea surface temperature
C_t	10^{-3}		Transfer coefficient
W	2	$\mathrm{m\,s^{-1}}$	Wind gustiness correction
T_{rw}	273.15	K	Reference temperature for water substance
P_{rw}	6.112	hPa	Reference pressure for water substance
T_{rd}	273.15	K	Reference temperature for dry air
P_{rd}	1000	hPa	Reference pressure for dry air
h_{rd}	0	$\mathrm{J\,kg^{-1}}$	Reference value for enthalpy of dry air
u_{rd}	0	$\mathrm{J\,kg^{-1}}$	Reference value for energy of dry air
s_{rd}	0	$\mathrm{J\,kg^{-1}\,K^{-1}}$	Reference value for entropy of dry air
h_{ri}	0	$\mathrm{J\,kg^{-1}}$	Reference value for enthalpy of ice
u_{ri}	0	$\mathrm{J\,kg^{-1}}$	Reference value for energy of ice
s_{ri}	0	$\mathrm{J\,kg^{-1}\,K^{-1}}$	Reference value for entropy of ice

Table 8.1: The constants in this table were arbitrarily chosen. Other constants used but not listed here, such as the latent heat at the reference points and the heat capacities, were taken from Emanuel (1994).

Smith's formula above this level:

$$P_v^*(T) = \begin{cases} 6.112\exp(17.67(T-273.15))/(T-29.65) & T < 273.15\text{K} \\ \\ \exp(23.33086 - 6111.72784/T + 0.15215\log(T)) & T > 273.15\text{K} \end{cases} \tag{8.3}$$

These formulas were taken from the book by Emanuel (1994), but the constants were modified, so the temperature, T, here is expected in degrees Kelvin. This equation gives the saturation vapor pressure in hecto-Pascals when T is the environmental temperature. On the other hand, by definition of dewpoint temperature, evaluating the above formula at the dewpoint gives the environmental vapor pressure.

Expressions of the key variables (moist energy, moist entropy, and the Bernoulli function) and their corresponding saturation deficits are derived in appendix A. The saturation deficit, which is a measure of the moisture in the environment, is plotted in figure 10.2.

Surface parameters are defined as their average over the first 20 m of the sounding. The temperature for the upper surface of the control cylinder is defined as the temperature corresponding to the minimum temperature in the sounding data. All these parameters are listed in table 8.2.

In order to combine sounding information with the results of the radar analysis, once all derived variables are estimated from the raw sounding data, the soundings (originally in their native resolution) are interpolated to 21 regularly spaced heights from the surface to the 20 km.

Table 8.2 Upper and Lower Boundary Parameters

Mission	Top	Surface Values						
Date	T_{top}	T	ρ	q_v	P_t	U_{eff}	$\mathcal{E}$	$\mathbf{J}_C$
	K	K	$\mathrm{kg\,m^{-3}}$	$\mathrm{g\,kg^{-1}}$	hPa	$\mathrm{m\,s^{-1}}$	$\mathrm{kg\,m^{-2}\,s^{-1}}$ $\times 10^{-5}$	$\mathrm{W\,m^{-2}}$
921126	187.25	301.65	1.22	16.97	1008.5	6.60	7.76	12.32
921128	189.35	302.35	1.22	16.65	1009.5	3.39	4.10	3.37
921212	184.35	300.45	1.21	14.75	1000.4	5.08	7.38	16.81
921213	181.75	301.35	1.21	16.62	999.0	5.84	7.23	12.96
921215	182.75	299.95	1.22	17.22	1006.7	8.52	9.84	34.05
930111	189.55	301.25	1.22	17.05	1010.2	3.22	3.74	7.63
930116	188.55	301.85	1.22	18.98	1006.8	6.32	5.93	10.27
930118	187.25	300.35	1.23	19.23	1005.9	5.67	5.19	19.93
930201	193.05	301.95	1.23	19.27	1010.0	7.64	6.84	11.50
930209	191.05	300.95	1.22	17.96	1007.2	4.92	5.23	13.52

Table 8.2: T_{top} is the temperature at the top of the control cylinder; T, ρ, q_v, P_t, and U_{eff} are the temperature, air density, vapor specific humidity, air pressure, and effective wind speed just above sea surface; $\mathcal{E}$ and $\mathbf{J}_C$ are the evaporation and conductive heat flux from the sea into the atmosphere.

Chapter 9

Mass Fluxes

Under the assumptions discussed in chapter 11 below, we may use the mass fluxes from a cloud system to estimate the fluxes of energy and entropy through the lateral boundary of a control cylinder that encloses the convection. Here we describe the steps required to estimate mass fluxes of a convective system using radial velocities sampled by a Doppler radar.

The first step to estimate the mass fluxes is the synthesis of the wind field from the raw radar measurements. This field is synthesized using the technique presented in section B.4. All cases presented here were processed in the following way: the flight level in-situ data were low-pass filtered with a smoothing length of 100 s before applying the automatic unfolding algorithm to the radial velocities; sea clutter was eliminated by discarding gates below 500 m; side lobe effects were reduced by eliminating gates within a 2000 m radius from the aircraft; the radar data were then interpolated to a Cartesian grid from the surface to the 20 km level with 5km $\times$ 5km $\times$ 1km grid spacing to generate dual-Doppler estimates of the Cartesian velocities. (See figure

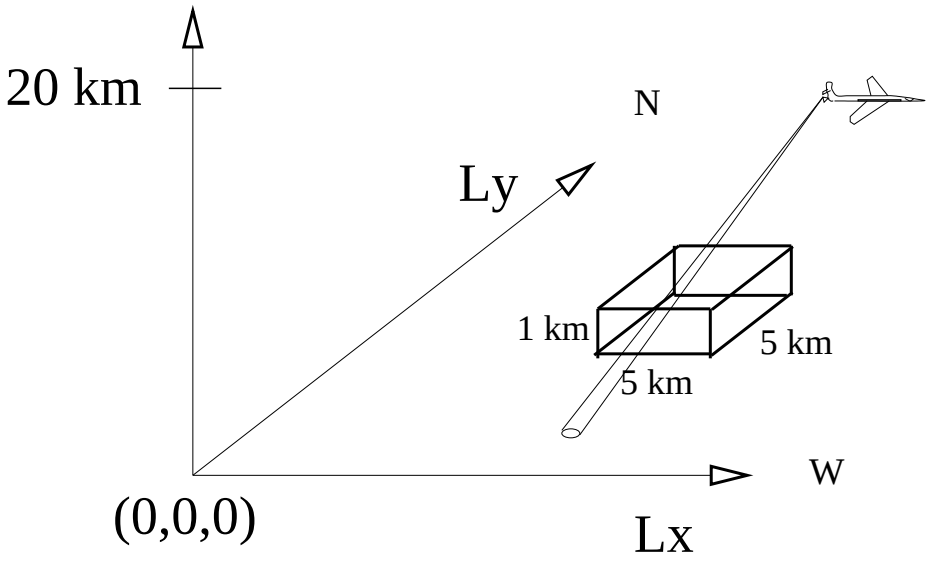

Figure 9.1: Interpolation grid for the cases presented here. The vertical height is always 20 km and the horizontal dimensions vary from case to to case in order to acomodate all radar data collected during the period of interest.

9.1.) The grid is fixed in the cloud system reference frame whose translation velocity was taken from Kingsmill and Houze (1999). Table 7.1 shows the information for the flight segments used to synthesize the wind field in each mission; grided data were discarded if the amplification of the error in Cartesian velocities due to the sampling geometry was larger than 1. Additionally to this threshold, grid points whose associated Cartesian speed was larger than 25 $\mathrm{m\,s^{-1}}$ were also discarded. The remaining velocities were fed to the anelastic mass continuity equation to generate estimates of the vertical velocities which were used to correct the dual-Doppler estimates of the horizontal velocities. Although the seemingly artificial threshold on speeds is not part of our regular interpolation technique, it is included here because histograms of the speeds from all the grid points made after applying the threshold on geometrical

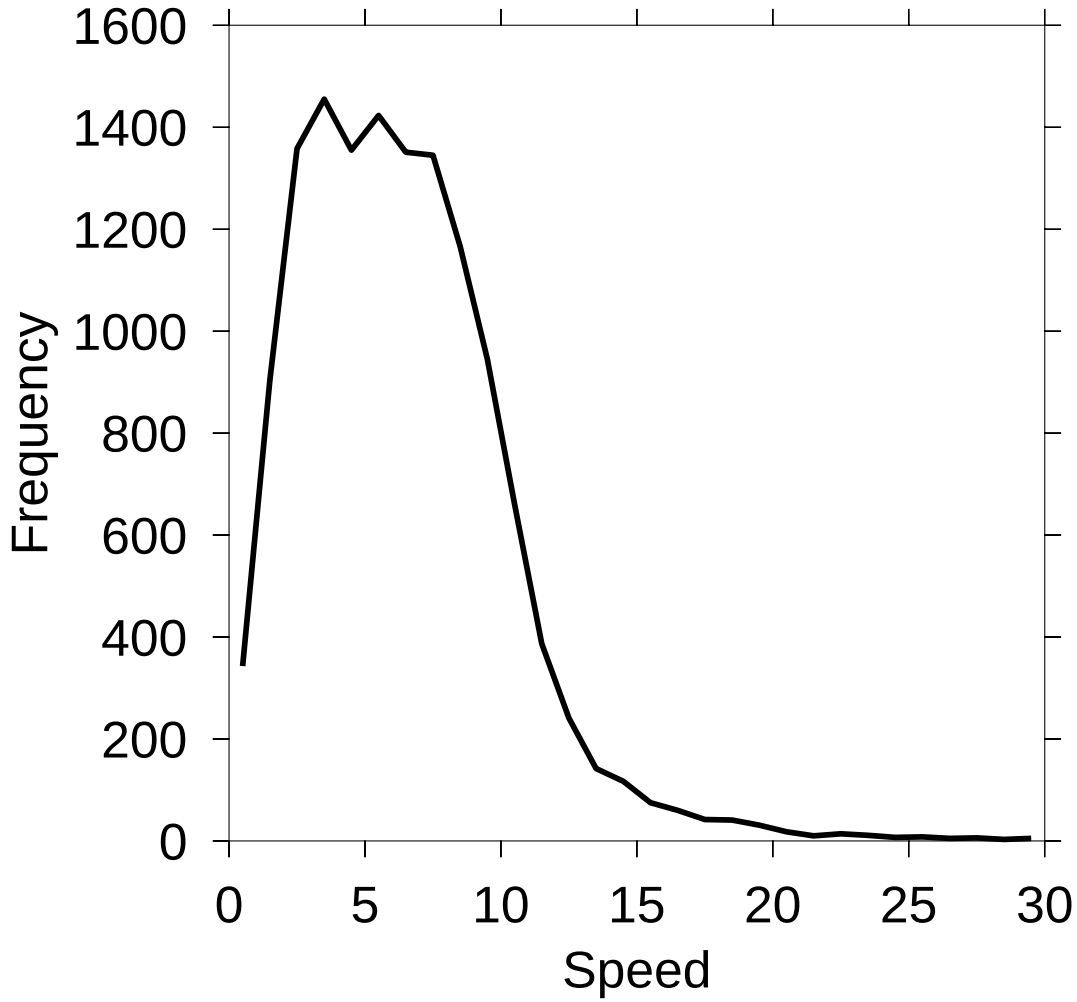

Figure 9.2: Histogram of Cartesian speeds for the case of December 15, 1992. This case corresponds to a deep convective system. All speeds from grid points where large geometrical errors (greater than 1 – see text) were not included in the histogram.

errors (figure 9.2) indicate that speeds larger than 20 $\mathrm{m\,s^{-1}}$ are indeed outliers, most probably due to isolated unfolding problems. The grid spacing may seem too big for the spatial resolution of the X-band radar measurements, which in the worst case is about 300 m in the radial direction and 1.6 km along the track. However, this grid spacing is still able to provide the major characteristics of the convective system, and

it is sufficiently large to accommodate enough radar data to make a robust interpolation. The characteristics and order of magnitude of the average mass fluxes do not change when we halve the grid spacing for any or all directions.

In the next step, the wind field is objectively analyzed to fill in holes and generate smooth mesoscale fields. Our objective analysis is performed as follows: An empty grid of the same size as that holding the Cartesian data is created. The value of a field (eg. reflectivity, velocity) at each point in this new grid is obtained by averaging all values of the same field inside a horizontal circle centered at the corresponding grid point on the original grid. For this average to be accepted, there has to be at least a minimum number of grid points inside the circle holding good data values of the field in question. If there are not enough good points, the value of this field is set to "bad" in the new grid. The radius of influence used during the smoothing process of the wind field was 30 km, and 15 good points had to be inside it in order to validate a point. After the smoothing process, a column-by-column divergence correction is applied. This correction is necessary because the objective analysis does not know about the conservation of mass at each individual column. Appendix D shows how this correction is done.

Finally, once the mesoscale wind field is obtained, the horizontal divergence, and hence the detrained mass flux, can be calculated. From there the vertical mass flux is obtained via the anelastic continuity equation.

Chapter 10

System Top and Tropospheric Moisture

We examine 10 cases out of the 25 where at least one WP-3D aircraft was present; see table 7.1. We chose these ten missions because all of them exhibit a clear convective behavior, judging from their vertical mass fluxes, and also because a sounding for the whole troposphere was made close, both in space and time, to the studied region. For this sample, we seek a correlation between cloud-system top height and tropospheric moisture. For this purpose, we employed the soundings prepared using the procedure given in chapter 8, and the mass fluxes obtained through the procedure described in chapter 9.

Cloud-system top height can be estimated in various ways from radar measurements. For instance, one method which has long been used is to simply take cloud-system top as the maximum height at which reflectivity is detected. We choose the maximum height of the average vertical mass flux as a surrogate for the cloud-system

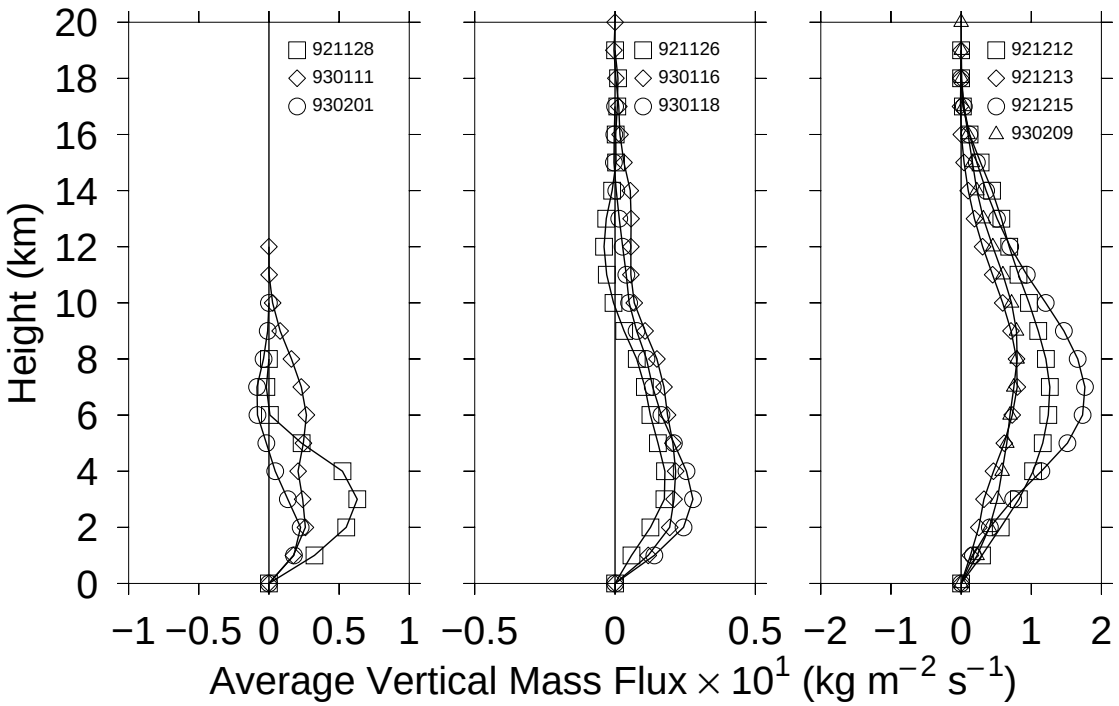

Figure 10.1: This figure shows the average vertical mass flux for the ten case studies examined here. They are grouped according to environmental moisture and cloud top height. Cases on the left panel correspond to small systems in dry environments. Tall systems in dry environments are in the central panel while tall systems in a moist environment are in the right panel.

top. Figure 10.1 shows the vertical mass fluxes for the selected ten case-studies. Since radars can only sense precipitation-sized particles, the cloud-system top obtained from radar measurements is always underestimated. Nevertheless, these measurements are still able to distinguish among systems by height, which is our primary interest.

From among the possible quantities which could represent tropospheric moisture, we have chosen the saturation deficits as measured by the difference between saturated and environmental moist energy, and moist entropy. These quantities are related to

the deficit in the mass fraction of water vapor (also known as the specific humidity), by the equations (A.5) and (A.12), respectively. On the other hand, the variations in such deficits are related to changes in moist entropy and energy, which (as shown in part one) play a key role in understanding moisture budgets. That is, for a given tropical environment, the saturated values of moist entropy and energy are constant; therefore, we can assume that variations in the saturation deficits are due to changes in the moist energy and entropy themselves. Actually, this is the reason for using these saturation deficits.

As figure 10.2 indicates, most of the moisture variability in the troposphere is below 10 km with the largest variations at mid-levels (4 km) and considerable variation close to the surface. Since the sounding values at the surface are not very reliable, we estimate the correlation in the layer from 1 kmto 10 km. Figure 10.3 shows this correlation. Since the selected layer practically includes most of the variability in the troposphere, this result indicates a quite good correlation between moisture in the troposphere and height of the cloud-system. Table 10.1 lists the values of moisture and height for these correlations as well as other characteristics of the cloud system obtained from the radar analysis.

We also performed a search to find a layer over which the average of the moisture correlates the best with the cloud-system top height. This search consisted in calculating the correlation coefficients among the 45 contiguous layers that can be formed with the sounding levels from 1 to 10 km (recall that the soundings were previously interpolated at 1 km intervals from the surface to the 20 km). The correlation coefficients between system-top height and moisture for the layers that give the best

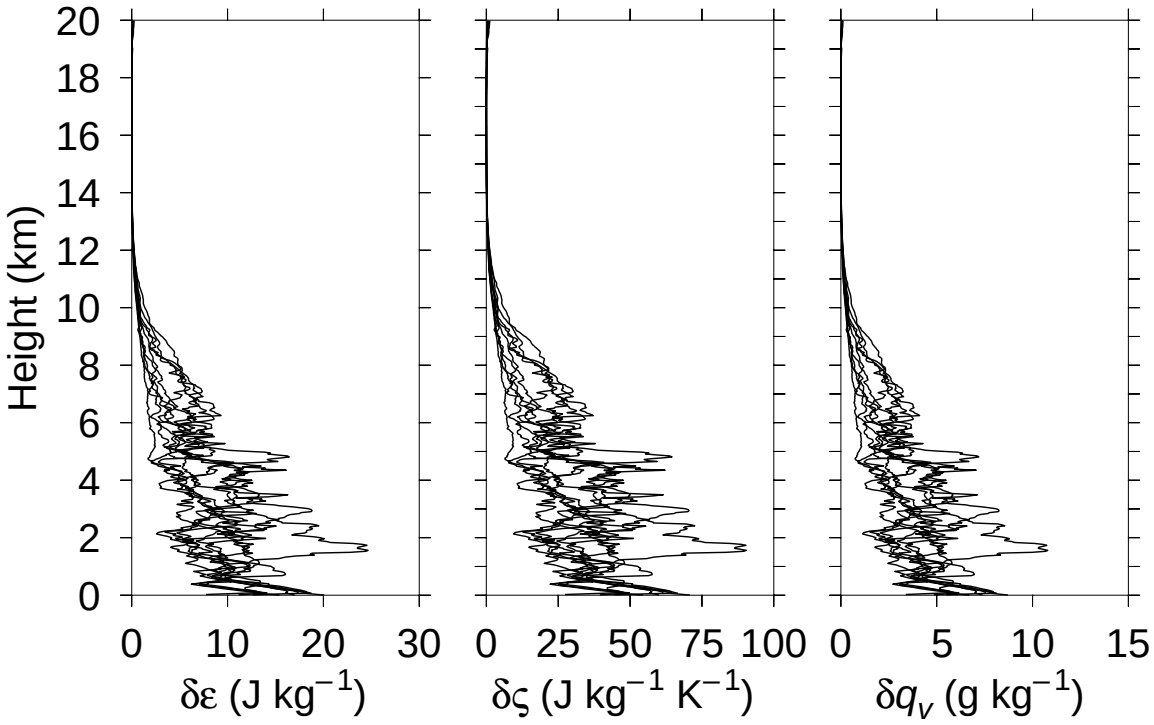

Figure 10.2: Vertical variation of the saturation deficits defined as the differences between saturated and environmental moist energy (left), moist entropy (center), and specific humidity (right), for all missions in this study.

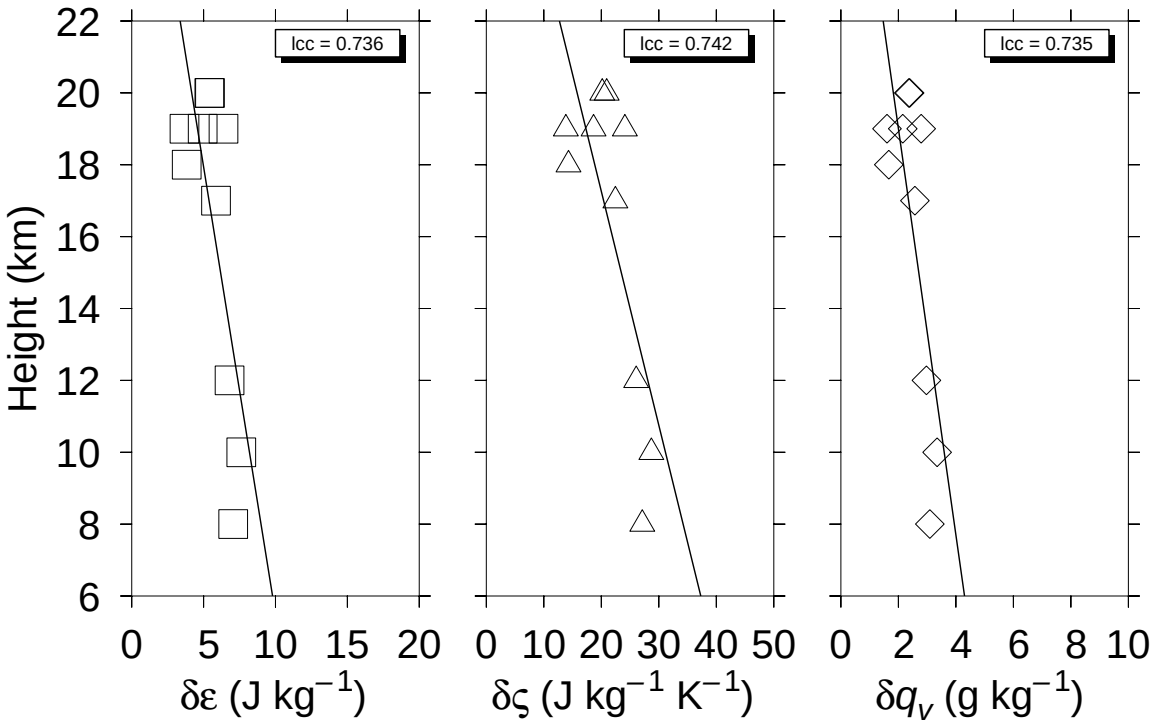

Figure 10.3: Correlation between system-top height and three measures of tropospheric moisture: In the left panel the moisture is represented by the moist-energy saturation deficit ($\delta\epsilon$), in the central by the moist-entropy saturation deficit ($\delta\varsigma$), and in the right by the specific-humidity saturation deficit (δq_v). In each case the saturation deficit is average over a layer extending from 1 km to 10 km. The corresponding correlation coefficients for each case are given at the top of each panel.

Table 10.1 Tropospheric Moisture and System Characteristics

Mission	$\overline{\delta\varepsilon}$	$\overline{\delta\varsigma}$	$\overline{\delta q_v}$	Z_{top}	A_{max}	D
Date	$(\mathrm{J\,kg^{-1}}) \times 10^3$	$(\mathrm{J\,kg^{-1}\,K^{-1}})$	$(\mathrm{g\,kg^{-1}})$	(km)	$(\mathrm{km^2}) \times 10^4$	(km)
921126	6.3873	24.0865	2.7942	19	78	3
921128	7.0624	27.1379	3.0913	8	8	3
921212	4.9382	18.6381	2.1534	19	30	7
921213	3.6681	13.8431	1.6041	19	51	7
921215	3.8184	14.2737	1.6704	18	36	7
930111	6.7995	26.0622	2.9783	12	17	2
930116	5.4361	20.9315	2.3899	20	29	4
930118	5.8594	22.4501	2.5759	17	40	2
930201	7.6272	28.7188	3.3477	10	30	1.5
930209	5.3980	20.1619	2.3633	20	58	8

Table 10.1: For each mission, the moisture in the environment is estimated using sounding data. Columns $\overline{\delta\varepsilon}$, $\overline{\delta\varsigma}$, and $\overline{\delta q_v}$ represent the average value from 1 km to 10 km for the saturation deficits of moist energy, moist entropy, and specific humidity, respectively. This table also shows some characteristics of the convective system obtained from the radar analysis: system-top height (Z_{top}); maximum horizontal area of the system (A_{max}); and depth of the inflow layer (D).

Table 10.2 Best Correlations

Layer (km)	$\delta\varepsilon$ v.s. Z_{top}	$\delta\varsigma$ v.s. Z_{top}	δq_v v.s. Z_{top}
3 – 5	0.7620	0.7680	0.7620
4 – 5	0.7520	0.7560	0.7520
2 – 10	0.7440	0.7460	0.7420
2 – 9	0.7420	0.7440	0.7410
1 – 10	0.7360	0.7420	0.7350

Table 10.2: The first column shows the layer over which the average of the corresponding saturation deficit was taken. The rest of the columns show the correlation coefficient for each correlation.

five results in our search are shown in table 10.2. These results show slightly better correlations with moisture at mid-levels, suggesting that the "moisture" interaction between clouds and environment is slightly favored at mid-levels. The correlation between cloud-system tops and mid-level moisture has been reported before in the literature; see for instance Brown and Zhang (1997) and Lopez-Carrillo and Raymond (1999).

Chapter 11

Lateral Export

In this chapter, we present a way to estimate the lateral export of moist energy and entropy using sounding and radar data.

Define χ to be either the moist entropy or the moist Bernoulli function. As shown in section 5.4, the export of these quantities through the lateral boundaries is given by

$$\int_{\mathsf{lat}} \rho \chi \mathbf{v}_d \cdot \hat{\mathbf{n}}_l \, da \tag{11.1}$$

where ρ is the air density and $\mathbf{v}_d$ is the dry air mean flow velocity. The integral is over the lateral boundary of the control cylinder, which should be big enough to include the convective system. This equation can be written as

$$\int_0^H \oint_c \rho \chi \mathbf{v}_d \cdot \hat{\mathbf{n}}_l \, dl \, dz \tag{11.2}$$

where the contour integral is over the curve c, which is the intersection between the lateral boundary and a horizontal plane; the z-integral extends from the sea surface to a height larger than the cloud-system top (see figure 5.1).

To estimate the value of this integral, we made the following assumptions:

1. The lateral boundary is far enough from the system to not be thermodynamically affected by the system. On the other hand, it is close enough that it responds dynamically to the presence of the system.

2. The convective system is the only source of divergence inside the lateral boundary.

3. Environmental values are homogeneous around the lateral boundary, so a sounding profile at any location on this boundary adequately represents all environmental characteristics at any other location over the boundary.

4. The horizontal velocity is the same for all components in the fluid.

The first assumption represents a situation where convective transport of energy and entropy have not had enough time to reach the lateral boundary, but on the other hand, gravity waves have reached the lateral boundary and established the flow pattern there. This assumption is generally satisfied as gravity waves travel much faster than air parcels. Typically gravity waves propagate with speeds between 20 and 50 $\mathrm{m\,s^{-1}}$, while air flow velocities are between 0 and 20 $\mathrm{m\,s^{-1}}$. The second assumption is not strictly satisfied. However, we can argue that the divergence associated with a convective system is larger than the environmental divergence. The third assumption is more difficult to sustain, particularly in reference to the moisture variability. However as figure (10.2) indicates, most of the moisture variability is concentrated below 10 km, with strong variations among the different cases at mid-levels (4 km).

Preliminary research (Lopez-Carrillo and Raymond, 1999) has shown that in a given environment, the relative humidity at mid-levels is nearly uniform over 600 km, and much of the remaining variation can be attributable to isolated rain showers. Finally, assuming that the horizontal velocities are the same for all components is the standard assumption in radar meteorology. Under these assumptions and using the Gauss's theorem for two dimensions, equation (11.2) may be rewritten as

$$\int_0^H \chi_e(z) \int_{A_C} \nabla_h \cdot (\rho \mathbf{v}_h)\, da\, dz \tag{11.3}$$

where $\chi_e(z)$ is the environmental profile of χ, $\nabla_h \cdot$ is the horizontal divergence operator, and $\mathbf{v}_h$ is the horizontal flow velocity. Since the only place inside the control cylinder where there is a source of divergence is the convective region, the area of integration, A_C, is equal to the horizontal extent of the convective system.

Defining the average detrained mass flux due to convection as

$$F(z) = \frac{1}{A_C} \int_{A_C} \nabla_h \cdot (\rho \mathbf{v_h})\, da \tag{11.4}$$

the export per unit volume through the lateral boundary of the control cylinder can be written as

$$\frac{A_C}{A\,H} \int_0^H \chi_e(z) F(z)\, dz \tag{11.5}$$

where H and A are the height and horizontal area of the control cylinder. Figure 11.1 shows the profiles of $F(z)$ for the ten case-studies selected in this research. Table 11.1 lists the lateral export corresponding to those case-studies.

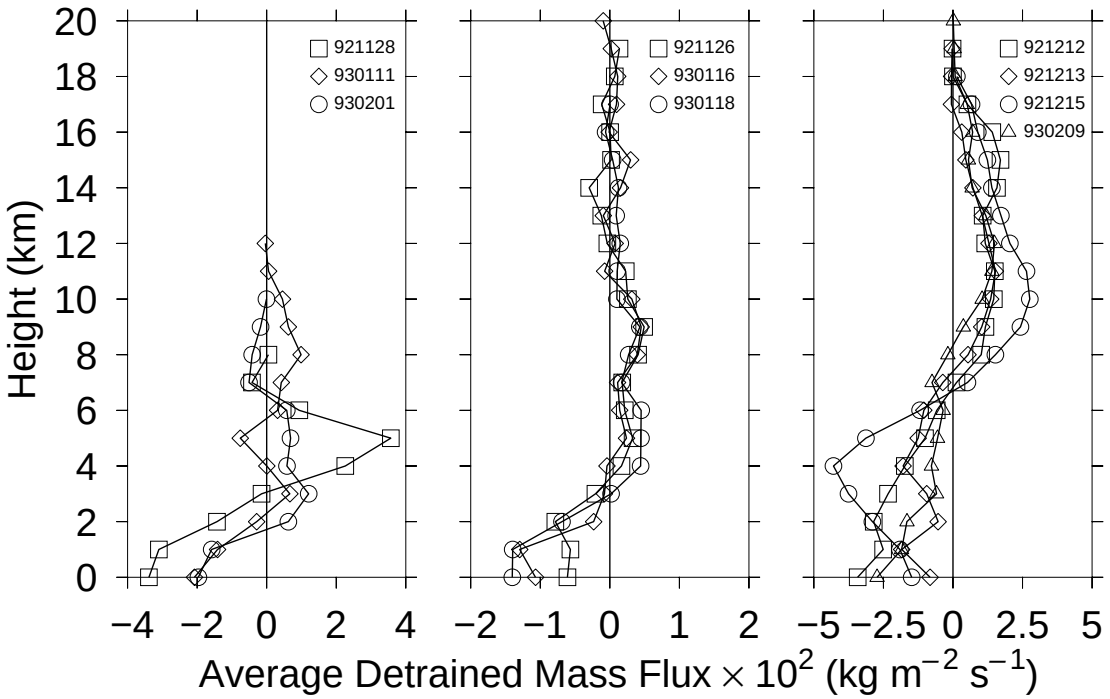

Figure 11.1: Average detrained mass flux for the ten case studies examined here, grouped according to environmental moisture and cloud top height. Cases in the left panel correspond to small systems in dry environments. Tall systems in dry environments are in the central panel; deep systems in a moist environment are in the right panel.

Lateral Export

Mission Date	ME ($W\,m^{-2}$)	Implied Role	MS ($W\,m^{-2}\,K^{-1}$)	Implied Role
921126	+ 79.8	?	+ 17.1	M
921128	+ 196.7	?	+ 79.4	M
921212	- 626.1	D	- 236.8	?
921213	- 266.0	D	- 96.6	?
921215	- 690.0	D	- 260.9	?
930111	+ 38.1	?	+ 17.9	M
930116	- 4.2	D	- 2.1	?
930118	+ 3.9	?	+ 4.7	M
930201	+ 137.8	?	+ 52.1	M
930209	- 404.6	D	- 164.0	?

Table 11.1: Convective contributions to the budgets of moist energy (ME) and moist entropy (MS), respectively. The implied role of the convective system over its environment according to the analysis presented in chapter 6 is also listed.

Conclusion

In this work, a correlation between cloud-top height and environmental moisture is found on a case-by-case basis. The environmental moisture is considered as a background or initial state of the atmosphere before the outbreak of convection. Even though an effort is made to insure that selected soundings are not contaminated by the presence of the system, this is not a solved issue. Therefore, it could be a major source of error. Assuming that environmental measurements of moisture are indeed used, it follows that deep convection requires a moist environment to occur, therefore, it is implied that it is the environmental moisture which controls the height of the clouds and not vice-versa.

In the effort to understand the role played by different convective regimes on environmental moisture, a theory to distinguish moistening from drying situations is developed. The novelty of this theory is that it does not depend on the highly uncertain precipitation rate. Even though the equations for energy and entropy used in this formulation do depend on unknown and difficult-to-estimate source terms, it is shown that estimations for these terms are not required to accomplish the goal of distinguishing between drying and moistening. The key assumption underlying the theory is that of small horizontal temperature gradients over the tropical atmosphere, where "small" means that the temperature can be considered as a constant on mesoscales. The accuracy of this assumption relies ultimately on observations. For the particular cases analyzed here, aircraft in-situ-measurements taken during ferry flights (4 km height) show a standard deviation of 0.5 K over 600 km . Though variability at other altitudes is unknown, it is not expected to have a severe impact on the conclusions. A theoretical analysis of such impact is missing at this point.

In order to distinguish drying from moistening situations, all but the source terms in the balance equations of energy, and all but the internal sources in the entropy balance, must be estimated. However, we have limited our data analysis to the estimation of the lateral export contribution to the tendency of the moisture equations. In order to quantify this contribution in concrete cases, it was necessary to make additional assumptions. Two of these assumptions are the more restrictive: small horizontal gradients of environmental moisture and zero environmental divergence. The gradient in environmental moisture has to be small enough so the moisture can be considered constant over mesoscales. During TOGA-COARE, ferry flights from Honiara to the studied regions showed that moisture is quite homogeneous over 600 km , with most of the variation due to individual convective clouds (Lopez-Carrillo and Raymond, 1999). The lack of data needed to estimate environmental divergence is surmounted by assuming that such divergence is small compared to the divergence due to convection.

Our results (see table 11.1, and figures 10.1 and 11.1) show that deep convective systems export energy and entropy, while small and/or weak convection has a tendency to import energy and entropy. Though limited, these results suggest that the role of deep convection is to dry its environment, while that of small and/or weak convection is to moisten it. Since deep convection requires a moist environment, it is also implied that convection evolves until it reaches a state of self-limitation.

In summary, the following conclusions are drawn from the analysis presented through out this work:

- A correlation between cloud-top and tropospheric moisture exists on a case-by-case basis.
- The moisture in the environment controls the height of the clouds and not vice-versa.
- Deep convective clouds dry their environment.
- Small clouds moisten their environment.
- Convection is self-limited.

Appendix A

Clear air sounding profiles

In addition to the primary variables of the sounding and specific humidities discussed in section 8, the moist energy, entropy and Bernoulli function, also depend on the temperature of the precipitation liquid water right before it reaches the sea surface. Unfortunately, this information is not contained in the sounding data. Thus, we must make an assumption about its value. We believe that a good approximation for this temperature is the value of the wet-bulb temperature at the surface, whose value can be obtained from dewpoint and the environmental temperature and pressure measured close to the surface. The isobaric wet-bulb temperature is defined by an implicit relationship (see for instance Emanuel, 1994) which can be solved numerically. We define the temperature of the liquid precipitation at the surface as the average of the isobaric wet-bulb temperature over the first 20 m of the sounding.

A.1 Moist energy

Among other things, the moist entropy depends on the total energy of precipitation liquid water at the sea surface ($e_{pl,b}$), which is assumed to be a constant in the analysis. Because the kinetic energy of precipitation is much smaller than its internal energy and its geopotential is zero at the sea surface, the total energy of precipitation is approximated to the value of its internal energy at sea surface: $e_{pl,b} = u_{lp,b}$. Furthermore, for a clear air balloon sounding, the kinetic energy of the jth component (just dry air and water vapor in this case) can be approximated as follows:

$$k_j = \frac{|\mathbf{v}_d|^2}{2}\left(1 + 2\hat{\mathbf{v}}_d \cdot \frac{\mathbf{v}_{Dj}}{|\mathbf{v}_d|} + \frac{|\mathbf{v}_{Dj}/|^2}{|\mathbf{v}_d|^2}\right) \tag{A.1}$$

where $|\mathbf{v}_d|$ and $\hat{\mathbf{v}}_d$ are the magnitude and unit vector of the dry air velocity velocity, respectively, and $\mathbf{v}_{Dj}$ is the diffusion velocity of the jth component. Since in clear air the velocity of dry air is approximately equal to the wind speed, which is much larger that the diffusion velocity of water vapor, and the vertical component of the wind velocity is also much smaller than the horizontal one, it follows that

$$k_j = \frac{v_h^2}{2} \tag{A.2}$$

where v_h is the horizontal wind speed, which is known from the sounding data. We could argue that this contribution to the total energy is very small compared to the internal energy of the components; however, it is kept because its value is directly measured by the balloon sounding instruments. Thus, for clear air balloon soundings, the moist energy can be approximated as

$$\varepsilon = v_h^2/2 + g\,z + q_d u_d + q_v u_v - q_v u_{lp,b} \tag{A.3}$$

where u_d, and u_v are the internal energies of dry air and water vapor, respectively.

Using equations (4.16),(4.17), and (4.18), the equation for moist energy can be written as

$$\begin{aligned} \varepsilon = v_h^2/2 + g\,z \quad &+ \quad q_d[c_{vd}\,(T_e - T_r)] + u_{dr}] + q_v[c_{vv}\,(T_e - T_r) + u_{vr}] \\ &- \quad q_v[c_l\,(T_{pl,b} - T_r) + u_{lr}] \end{aligned} \tag{A.4}$$

where u_{dr}, u_{vr}, and u_{lr} are internal-energy reference constants whose values are given by equations (4.20-4.22) and are listed in table 8.1; $T_{pl,b}$ is the temperature of the liquid precipitation just before it reaches the sea surface, which we choose to approximate by the wet-bulb temperature. The saturated value of the moist energy may be obtained from this equation by substituting the specific humidity for its saturated value. Therefore, the saturation deficit as measured by the moist energy can be written as

$$\delta\,\varepsilon = \delta q_v[u_v - u_d - u_{lp,b}] \tag{A.5}$$

where $\delta q_v = (q_v^* - q_v)$ is the saturation deficit measured by the specific humidity. From the above equation the proportionality between the saturation deficits measured by the specific humidity and moist energy at each level of the sounding can be seen. Figure 10.2 shows the profile of these measures of the environment's saturation.

A.2 Moist Bernoulli function

The quantity required to estimate the export of moist energy through the lateral boundaries in the moist energy budget (equation 5.21) is not the moist energy itself,

but the moist Bernoulli function given by equation (5.20). Since $b_{pl,b} = e_{pl,b}$, using the explicit expression for the Bernoulli function, equation (4.34), and the results of the previous section, the modified Bernoulli function for clear air can be written as

$$\Upsilon = \varepsilon + T(q_d R_d + q_v R_v) \tag{A.6}$$

where ε is the moist energy given by equation (A.4). The saturated value of the moist energy may be obtained from this equation by substituting the moist energy and specific humidities for their saturated values. Therefore, the saturation deficit as measured by the moist Bernoulli function can be written as

$$\delta\,\Upsilon = \delta\varepsilon + \delta q_v T(R_v - R_d) \tag{A.7}$$

where δq_v is the saturation deficit measured by the specific humidity. Since ε is proportional to δq_v, the moist Bernoulli function is also proportional to δq_v. A profile of this measure of the environmental moisture is given in figure 10.2.

A.3 Moist entropy

For clear air, the moist entropy is given by

$$\varsigma = q_d s_d + q_v s_v - q_v s_{pl,b} \tag{A.8}$$

where s_d and s_v are the entropies of dry air and water vapor, respectively, and $s_{pl,b}$ is the entropy of the liquid precipitation just before it reaches the sea surface. The explicit forms of s_d, s_v, and $s_{pl,b}$ are given by equation (4.37). According to that equation, the saturated values of these entropies can be written as

$$s_d^* \;=\; s_d + R_d \log(P_d/P_d^*) \tag{A.9}$$

$$s_v^* = s_v + R_v \log(P_v/P_v^*) \tag{A.10}$$

$$s_{pl,b}^* = s_{pl,b} \tag{A.11}$$

where P_d and P_v are the partial pressures of dry air and water vapor, respectively, and P_d^* and P_v^* their corresponding saturated values. Thus, the saturated value of the moist entropy can be written using these expressions plus the saturated value of the specific humidity in equation (A.8). The saturation deficit as measured by the moist entropy is given by

$$\delta\varsigma = \delta q_v(s_v - s_d - s_{pl,b}) + \log[(P_d/P_d^*)^{q_d^* R_d}(P_v/P_v^*)^{q_v^* R_v}] \tag{A.12}$$

A profile of this measure of the environmental moisture is given in figure 10.2.

A.4 Measurement Error

Given the following uncertainties in the measurements: pressure $\pm$ 0.1 hPa; temperature $\pm$ 0.2 K; dew point $\pm$ 0.5 K; and wind velocities $\pm$ 2 $\mathrm{m\,s^{-1}}$, the percentage error in the moist energy, Bernoulli function, and entropy are estimated to be about 3, 1, and 2 percent, respectively. These estimations where made using the following procedure: first we estimate the error in the derived variables (moist energy, Bernoulli function, and entropy) due to the measurement error in each of the primary variables (pressure, temperature, dew point, and wind speed), individually. For this purpose, we composed four artificial soundings in which one of the primary variables is modified by adding to it the uncertainty in its measurement while keeping the others untouched. These artificial soundings are then used to estimate the derived variables.

From here, the error associated with the individual uncertainties in the primary variables is obtained by taking the absolute value of the difference between estimates of derived variables using the actual and artificial data. Now, the total error due to all the uncertainties in the primary variables is taken as the sum of the individual errors associated with uncertainties in pressure, temperature and dew point and wind speed. The percentage value is simply 100 times the quotient of total error to the value of the derived variable calculated from the actual data. Finally, we repeat this process of finding total percentage errors for the selected soundings in this study and chose the biggest of them as our final estimation of the error in the derived variables.

Appendix B

Radar observations

B.1 Radar measurements in meteorology

For meteorological radar measurements, short pulses of coherent radiation concentrated in a very narrow beam are sent out from the antenna. When this radiation encounters cloud particles, it interacts with the molecules which scatter the radiation. Part of the scattered radiation goes back to the radar (backscatter radiation) and part goes forward (forward radiation). The duration, τ, of each pulse is about 1 μs, so typically each pulse is 300 m long. The beam size is characterized by the horizontal and vertical widths $\delta\theta$ and $\delta\phi$, respectively. These deltas are typically 1 degree, so when the pulse of radiation interacts with cloud, it will do so with a cloud volume defined by

$$V = \pi \frac{r\delta\theta}{2} \frac{r\delta\phi}{2} \frac{c\tau}{2} \tag{B.1}$$

This will be the sample volume. We have used $c\tau/2$ because the interest is on signals from the leading and trailing edge of the pulse that return to the radar exactly at the

same time, thus the leading edge can travel only a distance $c\tau/2$ before it starts its return trip; otherwise it would not arrive back at the radar simultaneously with echo from the trailing edge.

The sample volume typically contains a huge number of hydrometeors. For example, in continental clouds the concentration of precipitation-sized particles is on the order of a few to a few hundred raindrops per cubic meter and cloud droplet concentrations is about 200 cloud droplets per cubic centimeter, so typically the volume of the radar pulse is radiating something like 10^9 to 10^{12} raindrops and more than 2×10^{16} cloud droplets. Though the number of precipitation-sized particles is lower than the number of cloud droplets in a typical cloud they dominate the power return to the radar. This is because the effective backscatter cross section for small spherical targets increases with the sixth power of their diameter, see Doviak (1984) . The sum of the scattering cross sections of all scatterers within the sample volume per unit volume is called reflectivity. Besides the diameter of the scatterers, the cross section depends also on the wavelength of the radiation and the permittivity of the particle. Even though the permittivity is different for different kinds of scatterers (ice, liquid water, dust, etc..) it is normally taken as a constant. Therefore all the variation in the reflectivity will come from a factor that depends only on the geometry and amount of scatterers inside the control volume. This factor is called the equivalent radar reflectivity. This equivalent reflectivity is what weather radars normally report as reflectivity, and it is typically given in decibel units. Since the power returned to the radar by the scatterers is proportional to their scattering cross section, the reflectivity(or reflectivity factor) provides a way to locate heavy rain spots. However,

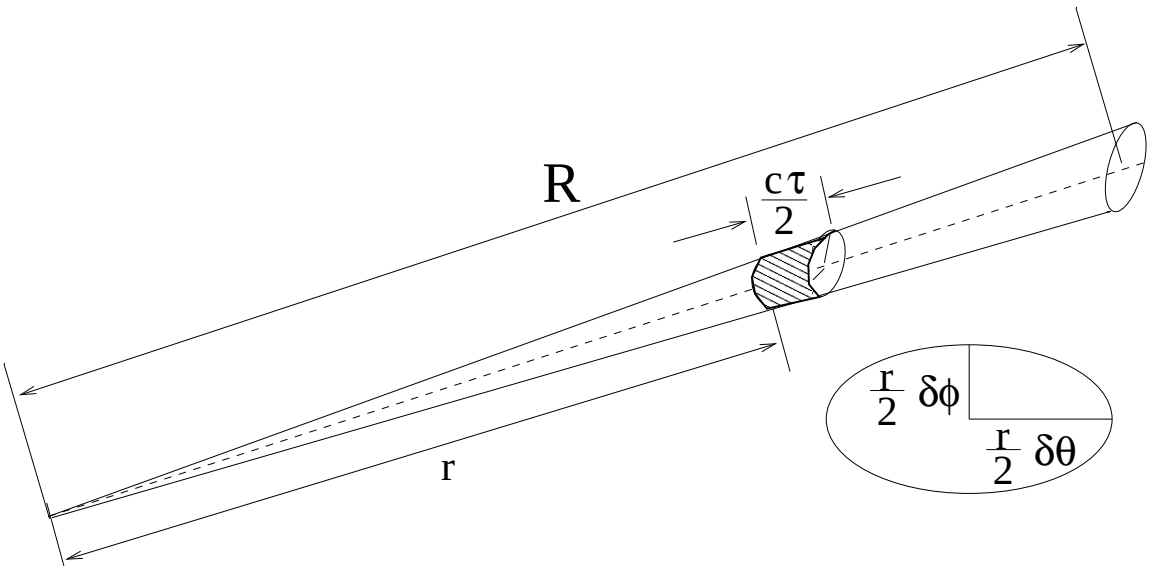

Figure B.1: Sketch of a radar ray showing one gate.

it is sometimes difficult to distinguish between situations with many small particles and those with fewer but larger particles.

The frequency at which the pulses are emitted from the antenna is called the Pulse Repetition Frequency (PRF). Therefore, the time between pulses is $T_s = 1/\text{PRF}$. This time is called the Pulse Repetition Time (PRT). Once a pulse is sent out, it can only travel a distance $cT_s/2$ in order for the backscatter radiation to be detected by the radar before the next pulse is sent out. We can think of this traveling pulse as forming a section of a radar ray. So a radar ray is formed from several radar volumes one after another. In this picture, radar volumes are called gates. Figure B.1 illustrates the situation. There will be $n = (cT_s/2)/(c\tau/2) = T_s/\tau$ gates per ray. While the antenna is not sending a pulse, it is busy receiving the backscatter radiation from the previous pulse and writing this information for the corresponding gate. There is a problem though — range ambiguity. Often, radars are operated with uniform

PRT, so that when targets have a range larger than $r_u = cT_s/2$, their echoes for the nth transmitted pulse are received after the $(n+1)$th pulse is transmitted (see figure B.2). Therefore, echoes from targets located beyond r_u will be confused with those coming from closer targets but from the $(n+1)$th pulse. Thus the actual range of a distant target will be folded into the interval $(0, r_u)$. Therefore, r_u is the range within which all targets must lie in order to have their range unambiguously measured. It should be noted that pulsed-Doppler radar can achieve useful and accurate measures of velocities for targets beyond r_u.

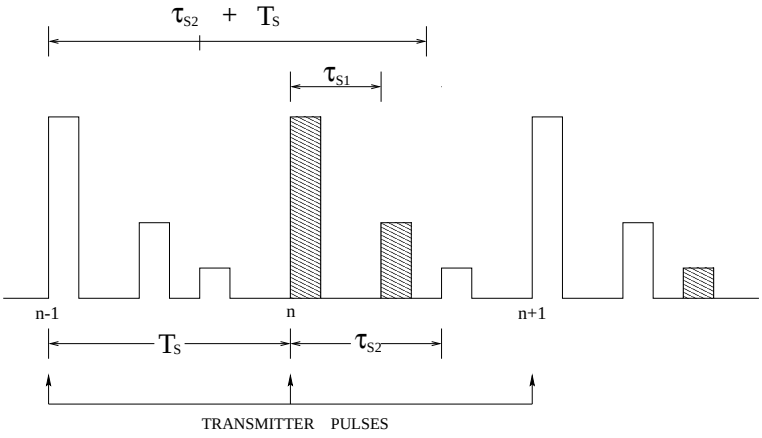

Figure B.2: Range-ambiguous echos. The nth transmitted pulse and its echos are crosshatched. This example assumes that the larger echo at delay τ_{s1} is unambiguous in range but the smaller echo, at delay τ_{s2}, is ambiguous. This "second-trip" echo, which has a true delay of $T_s + \tau_{s2}$, is due to the $(n-1)$th transmitted pulse. (Figure taken from Doviak (1984), pg. 45)

B.2 Doppler Radar measurements

Conventional, non-Doppler radars only measure the power received from a target. With Doppler radars, we are interested in measuring the radial velocity of the target relative to the radar, i.e. the speed of the target toward or away from the radar. To make this speed measurement, we need to measure the phase of the received signal compared to the phase of the transmitted signal, as well as the returned power. As with power-returned measurements, it can be shown (Houze, 1993) that Doppler measurements are biased towards the largest particles in the sample volume.

In the simplest configuration, we have a stationary radar observing moving targets. Each target that is moving will shift the frequency of the radar signal an amount which depends upon its speed toward or away from the radar. Let's consider a target at a distance r from the radar, so that the the round trip distance for waves received at the radar is $2r$. The phase of a wave is defined as

$$\phi = \omega t - \vec{k} \cdot \vec{r} + \phi_0 \tag{B.2}$$

where ω is the angular velocity, $\vec{k}$ is the wave vector, $\vec{r}$ is the position vector measured from the radar location, and ϕ_0 is the initial phase. Thus, the phase received at the radar ($\vec{r} = 0$) will be

$$\begin{aligned} \phi &= \omega \frac{2r}{c} + \phi_0 && \text{(B.3)} \\ &= \frac{2\pi c}{\lambda} \frac{2r}{c} + \phi_0 && \text{(B.4)} \\ &= \frac{4\pi r}{\lambda} + \phi_0 && \text{(B.5)} \end{aligned}$$

where c is the wave propagation speed and λ is the wavelength used for the radar.

Most meteorological radars operate at wavelengths of 3 cm (X-band), 5 cm (C-band) or 10 cm (S-band). The shorter wavelengths are more sensitive to weakly reflecting targets, but they suffer stronger attenuation by rain.

From equation (B.5), we can calculate the change of phase with time from one pulse to the next:

$$\begin{aligned} \frac{d\phi}{dt} &= \frac{4\pi}{\lambda}\frac{dr}{dt} \\ &= \frac{4\pi}{\lambda}V_r \end{aligned} \tag{B.6}$$

where V_r is the component of the target velocity along the radar beam. The rate of change of the phase is basically the total shift in frequency due to the velocity of the target detected at the radar location.

To compute this Doppler shift frequency for each radar volume (gate), the radar compares the phases of the electric field for consecutive pairs of pulses. The radar makes this calculation for several pairs and then averages all the results to yield a final estimate of the Doppler shift. This final estimate is substituted into (B.6) to obtain the estimate of the mean radial velocity .

As mentioned above, Doppler shift frequency is sampled at intervals $T_s = 1/\mathrm{PRF}$. Unfortunately, given a set of samples, we cannot relate them to one unique Doppler frequency. Figure B.3 shows that the same set of samples could have resulted from any one of the three signals having different Doppler frequencies. All such signals that fit the sample data set are called aliases, and $f_N = (2T_s)^{-1}$ is the Nyquist (or folding) frequency, which is the maximum frequency that can be detected for a given sampling rate. All Doppler frequencies between $\pm f_N$ are the principal aliases, and a frequency

higher than f_N will be folded into the interval $(-f_N, f_N)$, generating ambiguities. If

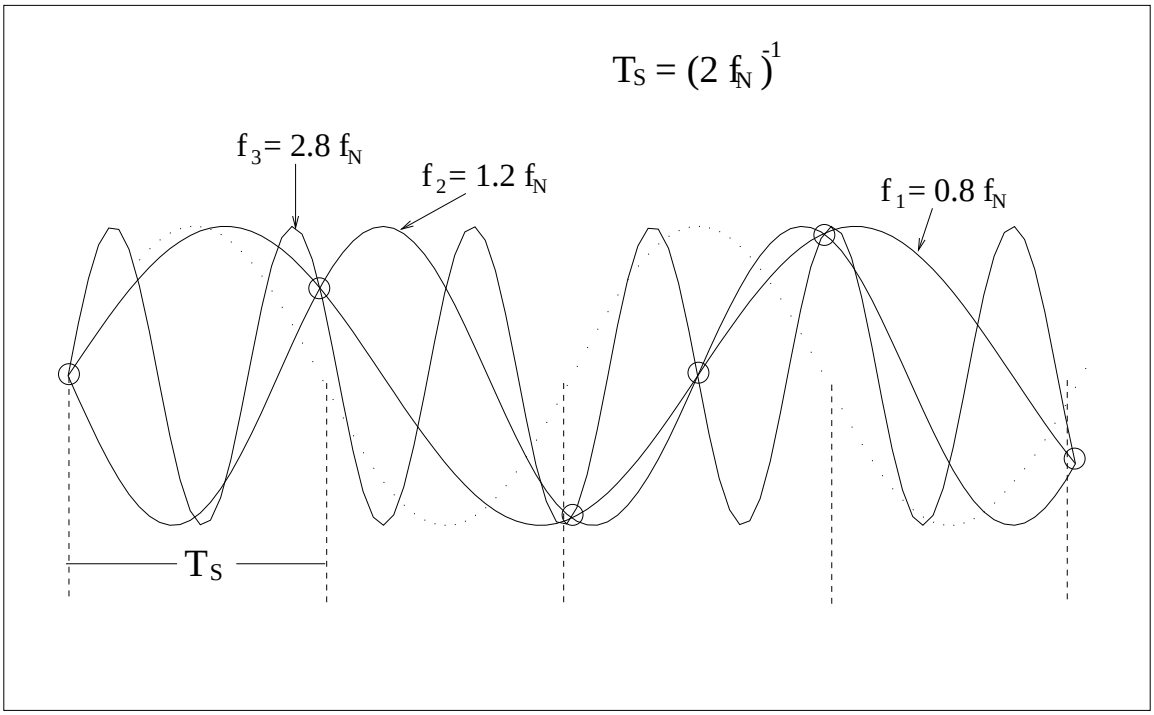

Figure B.3: Signals at three different Doppler frequencies that yield , when sampled, the same set of data. These Doppler frequencies are aliases of each other.(figure taken from Doviak (1984) pg. 45)

we use $2\pi f_N$ as the maximum unambiguous Doppler shift in equation (B.6), then we find that the maximum radial velocity that can be detected unambiguously is $V_N = \lambda/4Ts$. This threshold velocity is called the Nyquist velocity. So, V_r is unambiguously detected only in the interval

$$|V_r| \leq V_N \tag{B.7}$$

In principle we could increase V_N by increasing the PRF $(1/T_s)$. In so doing, however, we reduce the unambiguous range as was mentioned in section B.1.

There are now some techniques that involving the use of different radar wave-

lengths which serve to extend the unambiguous velocity. We will not go into those techniques here, since our radar data was sampled at a single wavelength of 3.22 cm. Some details about those techniques can be found in Doviak (1984), chapter 7 .

B.3 Airborne Doppler Radar

Airborne Doppler radar has proven very useful in providing information on meso- and convective- scale weather systems. It provides possibly the best observations of systems which are inaccessible to ground based radars, such as hurricanes. Airborne Doppler radar was particularly useful during TOGA-COARE, where the influence of land masses was not desired.

Even when radar parameters such as wavelength and PRT might be fixed, the flexibility of a mobile platform affords several ways to survey weather systems. Of importance to us are the scanning strategy (i.e. how the antenna itself is operated) and the aircraft trajectory used during the collection of the radar data. We illustrate some of the possible scanning and aircraft trajectory strategies in the following subsections.

B.3.1 Scanning strategy — FAST

The Doppler radar is mounted in the tail of the aircraft and has three axes of stabilization, allowing the radar system to position the antenna at a prescribed angle relative to the ground track of the aircraft. In addition, the radar has the ability of alternating the prescribed angle from sweep to sweep. The capability to alternate

angles between sweeps enables the radar to simulate a dual-beam radar, scanning one sweep forward, and one sweep aft– this fore/aft scanning technique is called FAST (see fig.B.4).

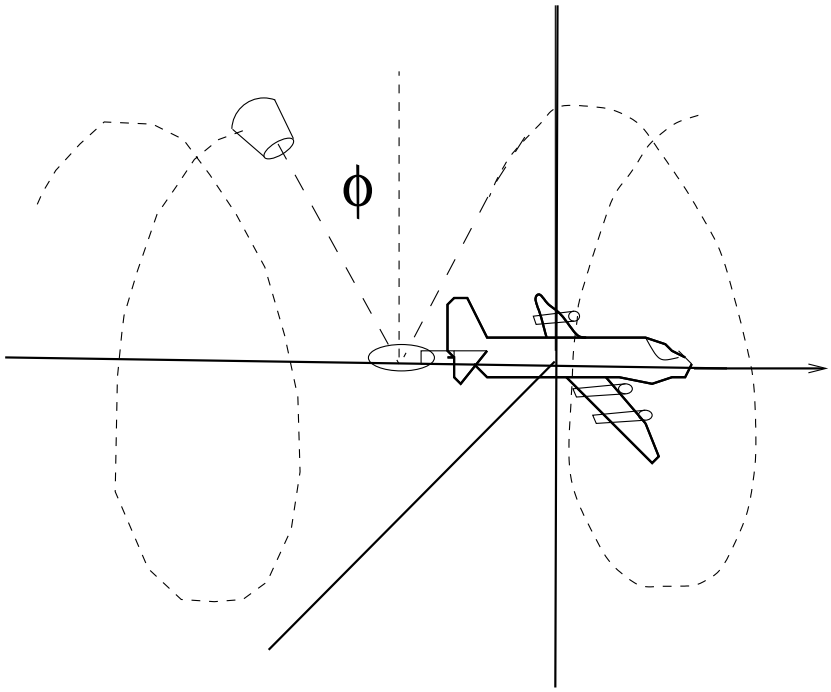

Figure B.4: Fore/Aft scanning technique (FAST)

FAST is implemented in such a way that the tail radar alternates between forward and aft sweeps, at a prescribed tilt angle measured off a perpendicular to the ground track($< 125°$). This allows the radar to sweep out two cones that intersect at various ranges from the plane's ground track, see figure B.5, which in turns provides pseudo-dual Doppler coverage without flying two different headings. Flying two different headings will provide multiple Doppler coverage. In the FAST continuous mode, the antenna sweeps a full 360° in the vertical plane at the prescribed rotation rate. For instance, at 10 RPM and aircraft ground speed of 140 m/s, each revolution would

be separated by 840 m, so in FAST continuous mode each revolution in the same pointing direction would be separated by 1600 m. Hence, in this example, the spatial resolution is roughly 1600 m.

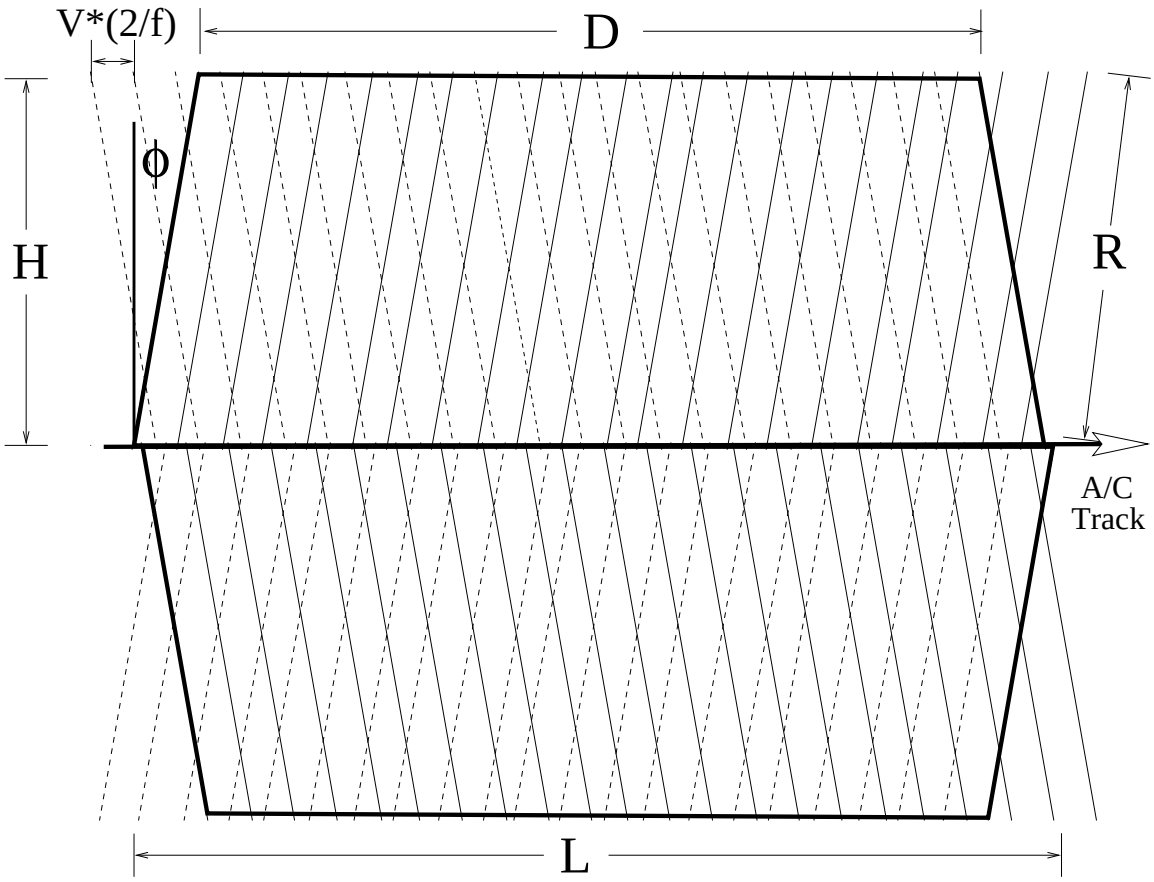

V Aircraft Velocity

f Antenna rotation rate

R Radar Range

L Length of the Aircraft Track

$H = R \cos(\phi)$

$D = L - 2 R \sin(\phi)$

ϕ Antenna Tilt Angle

Figure B.5: Horizontal pseudo-dual Doppler coverage for tail Doppler radar using the fore/aft scanning technique(FAST).

B.3.2 Trajectory strategies

FAST can be combined with many different aircraft trajectories. Although there are some general rules in designing aircraft trajectories — especially those concerning aircraft safety — in most cases aircraft trajectories are chosen by scientists in order to meet particular interests for the field experiment at hand. Figure B.6 shows two trajectories used during TOGA-COARE to survey convective systems.

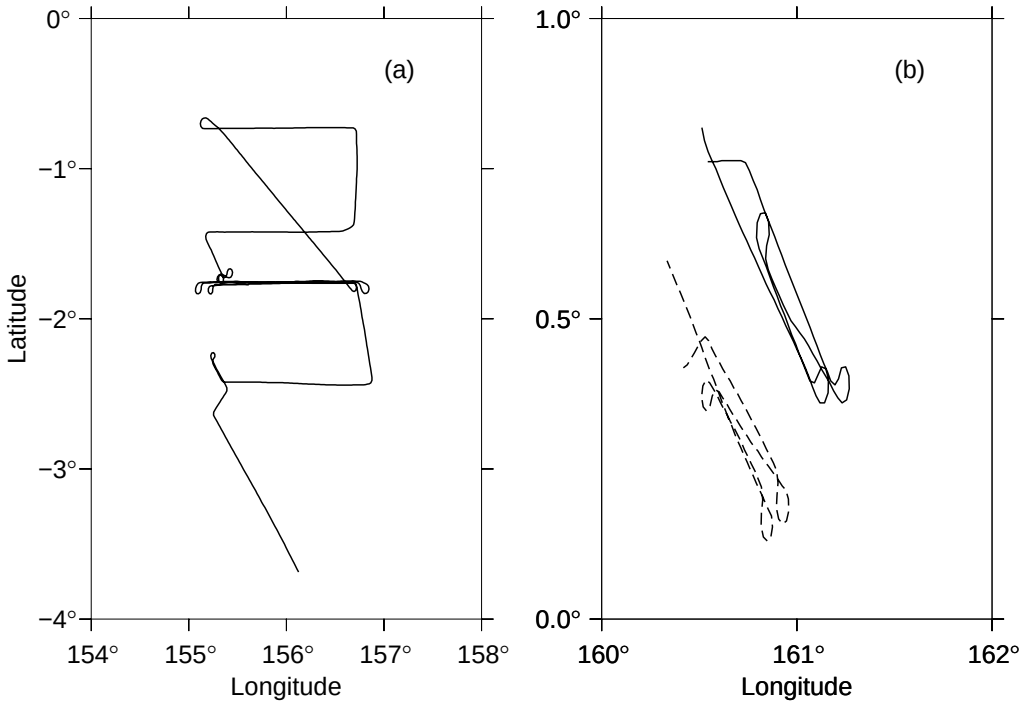

Figure B.6: Examples of aircraft trajectories used during TOGA-COARE to survey convective systems. Panel (a) shows a so-called "stack" flown by WP3-42 on February 1, 1993. Panel (b) shows part of the mission flown by WP3-43 (dashed) and WP3-42 (solid) on December 12, 1992. The segments were time-coordinated to allow for a more dense sampling. This sampling geometry performed by two aircraft in FAST mode is called quad-Doppler.

B.4 Wind field synthesis

In meteorology, a number of conclusions can be drawn just from knowing whether a cloud system is moving toward or away from a certain location. However, the kinematics of a given convective system is best studied (or at least, it is more straightforward to study) if we possess the wind velocity field of the system. Even though there are instances when some characteristics of the cloud system can be obtained directly from radial velocities – most remarkably the estimation of divergence profiles using an ad-hoc aircraft trajectory know as "purls" (Mapes 1992) – it is common practice to obtain the wind field before we start the analysis of the kinematics of the system. Normally, it is understood that this field consists of the Cartesian velocities of the wind at every point in a grid that covers the observed features of a cloud system. There are in the literature several techniques for constructing this field from Doppler velocities. Many of them are still a matter of ongoing research within the Doppler community. In this section, we present in some detail a technique pioneered by Raymond and Lewis (1995) , and further refined in Raymond, Lopez, and Lopez (1997). Though improvement of this technique is part of our current research, we present it here as it was used to synthesize the wind field of the ten case-studies reported in this work. Those cases were observed by the WP3 aircraft during TOGA-COARE; details are presented in part I.

Because the radar is moving while collecting data, the observed target velocity is a combination of the actual target velocity and the component of the aircraft velocity along the radial direction. Hence, the first step in the synthesis of the wind field is to

eliminate the aircraft velocity from the data as well as to correct for possible foldings in the target velocity. For this purpose, we employed an unfolding algorithm which uses the wind speed and navigation parameters from the flight level in-situ data of the corresponding aircraft. The idea behind the unfolding algorithm is that the velocities measured by the radar for parcels close to the aircraft have to be close to the velocity measured by the in-situ instruments. So, the radial velocity on the first gate of the radar ray is adjusted to be inside a Nyquist interval centered at the value of the in-situ measurement. Velocities for the rest of the gates are modified by assuming continuity along the ray. For instance, the velocity on a given gate has to have a value inside the Nyquist interval that is centered on the velocity of the previous gate. If it does not, it is adjusted by adding or subtracting an integer multiple of the Nyquist velocity. Note that this algorithm removes aircraft speed automatically.

The next step in the technique is to eliminate data that might be contaminated by sea clutter and side-lobe radiation from the antenna. Sea clutter is minimized by eliminating gates below a certain altitude. Reduction of side lobe effects is done by eliminating gates within a specified radius from the aircraft.

Subsequently, the remaining radar data are corrected for the Earth curvature and then re-navigated to a common reference frame moving with the storm. The re-navigation is a very important step in the analysis because we hope to generate a snap-shot of the system with the collected data, so we want to account for some of the evolution during the collection time. Furthermore, an inertial reference frame moving with the system is what we need to explore the true inflow-outflow characteristics of a given system. Note however, that velocities remain earth-relative during this process.

At this point, we are ready for the interpolation of the radial velocities to a Cartesian grid. Consider Figure B.7. Our problem is to estimate the velocity of the wind

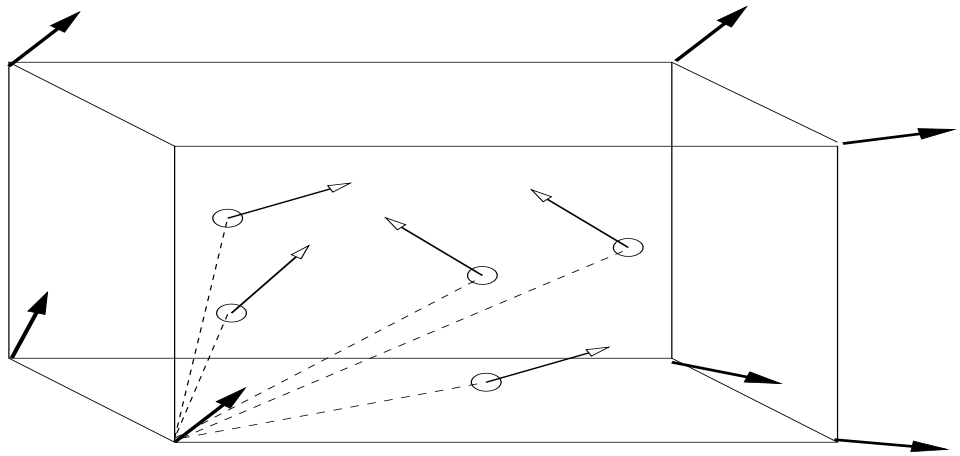

Figure B.7: Radial velocity measurements inside a grid volume. The spheres represent radar-sample volumes (i.e. gates). Arrows at the corners represent the interpolated wind velocities.

field $\vec{v} = (u, v, w)$ at every grid point, based on radar observation of the precipitation particle velocity $\vec{v_p} = (u, v, w_p)$, where we have assumed that the precipitation particles move with the wind velocity in the horizontal. On the other hand, the vertical particle velocity, w_p, is related to wind vertical velocity, w, by the equation

$$w = w_p + w_t \tag{B.8}$$

where w_t is the particle terminal velocity, which can be determined independently (for instance, from reflectivity measurements). Since radar can only detect radial velocities, our measurements are the projections of $\vec{v_p}$ over the radar-pointing direction, $\vec{n}$, i.e. $v_r = \vec{n} \cdot \vec{v_p}$. So, the information for each of the n measurements can be written

as

$$\begin{pmatrix} \cos(\theta_i) & \cos(\phi_i) & \cos(\gamma_i) \end{pmatrix} \begin{pmatrix} u & v & w_p \end{pmatrix}^T = \begin{pmatrix} v_{ri} \end{pmatrix} \tag{B.9}$$

where $\cos(\theta_i), \cos(\phi_i), \cos(\gamma_i)$ are the antenna cosine directions for the ith measurement, and $(u\ v\ w_p)^T$ is the transpose of the particle velocity. Equation (B.9) defines what is known as a forward problem where, given the cosine directions, if we know the Cartesian components of the velocity vector, then we can calculate the measured value of the radial velocity. So, our interpolation scheme is cast as the inverse problem, where we are given the cosine directions plus the radial velocities and we want the Cartesian components of the particle velocity. For $(n > 3)$, equation (B.9) is an over-determined system , so there is no exact solution, unless $n - 3$ of the equations are linearly dependent and can thus be eliminated. Further refinement to the interpolation scheme is made by giving more weight to measurements made closer to the interpolation point. So, in general, the weighted interpolation scheme becomes

$$\begin{pmatrix} h_i \cos(\theta_i) & h_i \cos(\phi_i) & h_i \cos(\gamma_i) \end{pmatrix} \begin{pmatrix} u & v & w_p \end{pmatrix}^T = \begin{pmatrix} h_i v_{ri} \end{pmatrix} \tag{B.10}$$

where $h_i = h_i(s)$ represents the weight for the ith measurement, and s is the distance between the interpolation and measurement points. In particular, for our data analysis the weight for the ith-measurement contributing to a grid point is given by

$$h_i = \frac{1/s_i}{\sum_{k=1}^{n} 1/s_k} \tag{B.11}$$

where s_i is the distance between the grid and measurement points and n is the number of all measurements made inside a grid box centered at the grid point. The contribution from measurements outside this grid box is defined as zero.

Inversion of equation (B.10) results in what is called a triple Doppler estimate for $\vec{v_p}$. However, such a solution is typically quite inaccurate when none of the ray's contributing gates to the grid point have a high elevation angle. In this case a dual Doppler solution may be attempted. For this synthesis, equation (B.10) is still applicable but because of the small elevation angles we do not trust the term $\cos(\gamma_i)w_p$. Instead of just getting rid of it, equation (B.10) is rewritten as

$$\begin{pmatrix} h_i\cos(\theta_i) & h_i\cos(\phi_i) \end{pmatrix} \begin{pmatrix} u & v \end{pmatrix}^T = \begin{pmatrix} h_i v_{ri} - h_i\cos(\gamma_i)w_p \end{pmatrix} \tag{B.12}$$

Since $(u\,v)^T$ will depend on w_p, a model is proposed to explicitly take this into account: Let

$$\vec{v_H} = \vec{v_{H0}} + \vec{f}w_p \tag{B.13}$$

where $\vec{v_H} = (u\ v)^T$ is the horizontal wind velocity, $\vec{v_{H0}}$ is the horizontal wind velocity when $w_p = 0$, and $\vec{f}$ is a constant vector to be determined. With this model our Doppler interpolating scheme becomes

$$\begin{pmatrix} h_i\cos(\theta_i) & h_i\cos(\phi_i) \end{pmatrix} \begin{pmatrix} u + f_x\ w_p \\ \\ v + f_x\ w_p \end{pmatrix} = \begin{pmatrix} h_i v_{ri} - h_i\cos(\gamma_i)w_p \end{pmatrix} \tag{B.14}$$

Defining the system matrix as

$$G = \begin{pmatrix} h_1\cos(\theta_1) & h_1\cos(\phi_1) \\ \\ h_2\cos(\theta_2) & h_2\cos(\phi_2) \\ \\ h_3\cos(\theta_3) & h_3\cos(\phi_3) \\ \vdots & \vdots \\ \\ h_n\cos(\theta_n) & h_n\cos(\phi_n) \end{pmatrix} \tag{B.15}$$

Equation (B.14) can be written as

$$G(\vec{v_{H0}} + w_p\vec{f}) = A - Bw_p \tag{B.16}$$

where

$$A = \left(\begin{array}{ccccc} h_1 v_{r1} & h_2 v_{r2} & h_3 v_{r3} & \cdots & h_n v_{rn} \end{array} \right)^T \tag{B.17}$$

$$B = \left(\begin{array}{ccccc} h_1 \cos(\gamma_1) & h_2 \cos(\gamma_2) & h_3 \cos(\gamma_3) & \cdots & h_n \cos(\gamma_n) \end{array} \right)^T \tag{B.18}$$

In order to obtain $\vec{v_{H0}}$ and $\vec{f}$, we start by multiplying both sides of equation (B.16) by G^T. This yields the normal equations for the system:

$$G^T G(\vec{v_{H0}} + w_p\vec{f}) = G^T(A - Bw_p) \tag{B.19}$$

Now, the solution for $\vec{v_{H0}}$ can be obtained by setting $w_p = 0$ in (B.19):

$$\vec{v_{H0}} = (G^T G)^{-1} G^T A \tag{B.20}$$

Substituting this result back into (B.19) gives

$$G^T G\vec{f} = -G^T B \tag{B.21}$$

from which we find

$$\vec{f} = -(G^T G)^{-1} G^T B \tag{B.22}$$

Note that $\vec{f}$ does not depend on velocity data. So far, we have estimates for the horizontal wind velocities $\vec{v_H}$, which depend on the dual Doppler estimates $\vec{v_{H0}}$ and the vertical particle velocity w_p.

The particle vertical velocities are obtained in the following way: First, the wind's vertical velocities are calculated from the horizontal velocities $\vec{v_{H0}}$ by a forward integration of the anelastic mass continuity equation, starting at the top of the cloud and

assuming zero vertical velocity at cloud top. (Details of the integration procedure are describe in Lopez-Cavazos (1995)). The particle terminal velocity is then estimated using the procedure in Jorgensen, LeMone, and Jou (1991), which is valid for the deep tropics – the particle terminal velocity is taken as negative, reflecting the downward motion of particles. Finally, the particle vertical velocities are computed as the sum of the vertical wind and the particle terminal velocity. At this point, equation (B.13) is used to calculate corrected values of the horizontal velocities. However, before we obtain the vertical velocities from horizontal velocities, we must eliminate bad horizontal velocities that arise during the synthesis of $v_{H0}^{\rightarrow}$. In the next section we illustrate how these bad estimations arise and how we handle them.

B.4.1 Error analysis

As mentioned in the previous section, the sampling geometry used to retrieve the radial velocities is not appropriate to obtain good estimations of the vertical component of the velocity. In general, if the angle between the radar ray and the velocity of the hydrometeors is close to 90°, then the retrieved value of the radial velocity will be close to the noise level. If all of the measurements that contribute to a Cartesian component of the velocity at a grid point have values at or below the noise level, we say that the component is not well resolved and must be eliminated from the analysis. This is especially critical for horizontal components of the velocity, if we are to use them to obtain the vertical component.

Since at the beginning we do not know what is the actual direction of a particle

motion, we can not settle for directly calculating the angle between that direction and the direction in which the radar beam is pointing (we do know this direction from the radar data). We approach the problem of identifying grid points with badly resolved Cartesian components by examining how the error in the measurements is propagated to the Cartesian fields. In what follows, we use the results derived in appendix C.

First, let's calculate the covariance matrix of $\vec{v_H}$. From equation (B.13), we have

$$cov(\vec{v_H}) = cov(\vec{v_{H0}} + \vec{f}w_p) \tag{B.23}$$

$$= cov(\vec{v_{H0}}) + cov(\vec{f}w_p) + 2cov(\vec{v_{H0}}, \vec{f}w_p) \tag{B.24}$$

where we have used equation (C.7). The covariance of $\vec{v_{H0}}$ can be obtained from equation (B.20)

$$cov(\vec{v_{H0}}) = cov((G^T G)^{-1} G^T A) \tag{B.25}$$

where $A = (h_1 v_{r1} \quad h_2 v_{r2} \quad h_3 v_{r3} \quad \cdots \quad h_n v_{rn})^T$ is the weighted data vector, and G is the system matrix given by equation (B.15). Equation (B.25) can also be written as

$$cov(\vec{v_{H0}}) = cov((G^T G)^{-1} g^T V_R) \tag{B.26}$$

where

$$g^T = \begin{pmatrix} h_1^2 \cos(\theta_1) & h_2^2 \cos(\theta_2) & h_3^2 \cos(\theta_3) & \cdots & h_n^2 \cos(\theta_n) \\ h_1^2 \cos(\phi_1) & h_2^2 \cos(\phi_2) & h_3^2 \cos(\phi_3) & \cdots & h_n^2 \cos(\phi_n) \end{pmatrix} \tag{B.27}$$

and $V_R = (v_{r1} \; v_{r2} \; v_{r3} \; \cdots \; v_{rn})^T$ is the unweighted data vector. Thus using (C.5), equation (B.26) can be written as

$$cov(\vec{v_{H0}}) = (G^T G)^{-1} g^T cov(V_R)[(G^T G)^{-1} g^T]^T \tag{B.28}$$

For radial velocity measurements, it is assumed that they all are independent and have the same standard deviation, so

$$cov(V_R) = var(V_R) I_{nxn} \tag{B.29}$$

where I_{nxn} is the $n \times n$ identity matrix. Then we have

$$cov(\vec{v_{H0}}) = (G^T G)^{-1} g^T \, g[(G^T G)^{-1}]^T var(V_R) \tag{B.30}$$

On the other hand, using equation (C.8) the variance of the second term in equation (B.24) can be written as

$$var(\vec{f} w_p) = \vec{f}\vec{f}^T var(w_p)) \tag{B.31}$$

Thus, the covariance matrix for $\vec{v_H}$ can be written as

$$cov(\vec{v_H}) = (G^T G)^{-1} g^T g[(G^T G)^{-1}]^T var(V_R) + \vec{f}\vec{f}^T var(w_p)) + 2cov(\vec{v_{H0}}, \vec{f} w_p) \tag{B.32}$$

The variance of $\vec{v_H}$ comes from the diagonal elements in (B.32).

$$\sigma^2_{v_{xH}} = \Psi_x \sigma^2_{V_R} + f_x^2 \sigma^2_{w_p} + 2cov(v_{xH0}, f_x w_p) \tag{B.33}$$

$$\sigma^2_{v_{yH}} = \Psi_y \sigma^2_{V_R} + f_y^2 \sigma^2_{w_p} + 2cov(v_{yH0}, f_y w_p) \tag{B.34}$$

where Ψ_x and Ψ_y are the diagonal elements of the matrix $(G^T G)^{-1} g^T g[(G^T G)^{-1}]^T$.

At this stage of development our technique focuses not on the actual value of the variance, but on how much this variance is affected by the geometrical configuration (angle between the direction of radar's ray and meteor's velocity) during the collection of the data. This configuration is buried in the coefficients Ψ_x, Ψ_y, f_x, and f_y. From equations (B.33) and (B.34), we see that contributions to the total error can be amplified, depending on the values of Ψ_x, Ψ_y, f_x, and f_y. So, we can set some

threshold for these amplification factors, such that we can discard grid points where thresholds are exceeded.

It is worth noting that such thresholds can be set even before we know the particle vertical velocity. This is very useful, because w_p is calculated based on the horizontal velocities via the continuity equation.

As an illustration of this procedure, let's consider the case of December 15, 1992. The data were taken by the X-band Doppler Radar mounted on the tail of the NOAA(National Oceanic and Atmospheric Administration) WP3-42. The antenna was used in FAST continuous mode to allow for a Doppler resolution of roughly 1.6 km. Radial velocities were interpolated to a Cartesian grid extending from the surface to 20 km, with 1 km intervals and horizontal grid size of 5 km, using the procedure described in section B.4.

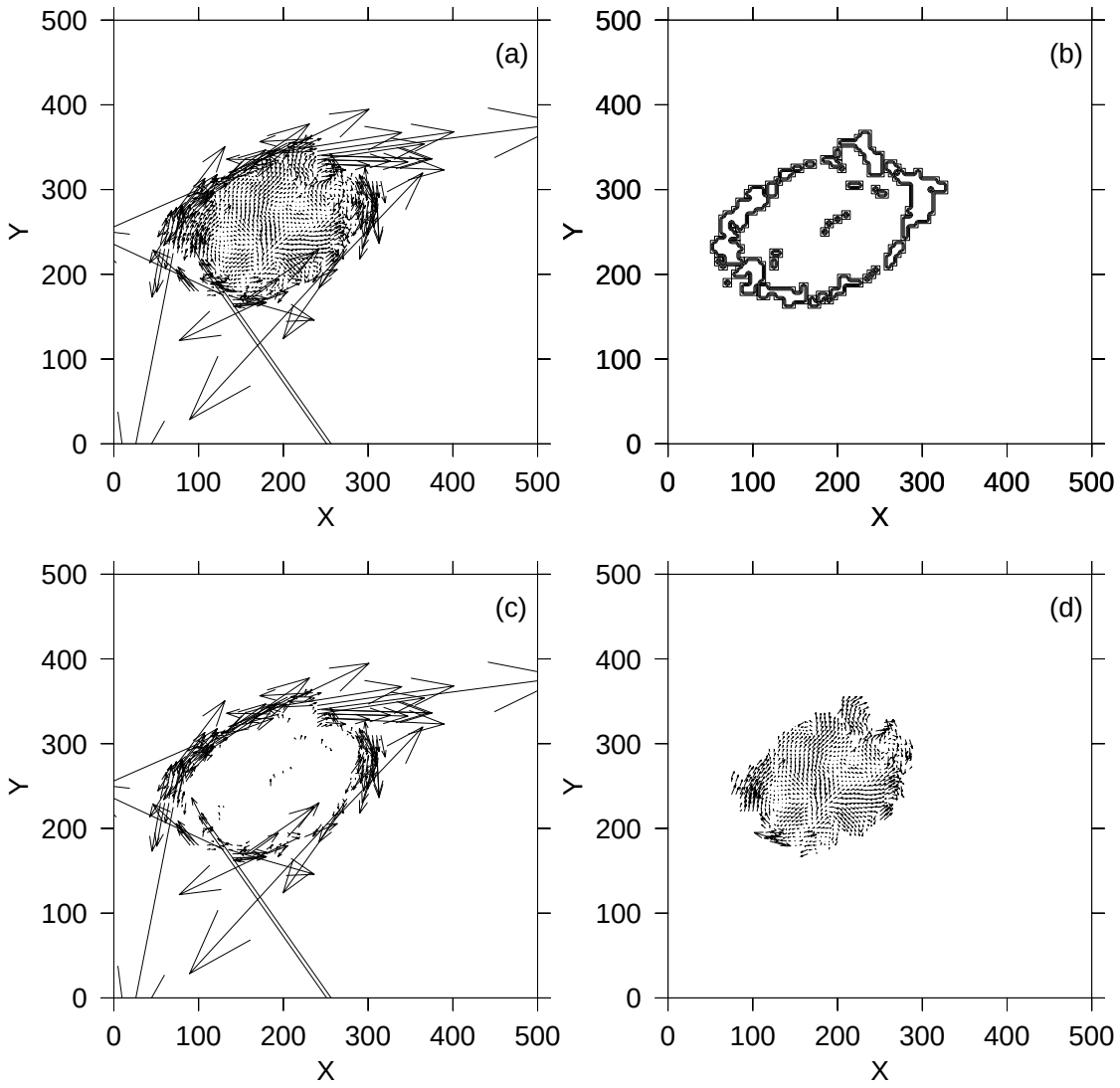

Figure B.8: Horizontal wind velocities assuming zero vertical particle velocity for the case of December 15, 1992, surveyed by the WP3-42 during TOGA-COARE. The velocities are Earth-relative, but they are shown in the storm reference frame. The axes are NS-EW oriented and their scale is in km . The arrow scale is 1 km per 1 $\mathrm{m\,s^{-1}}$. All panels refer to the 10 km height. (a) All velocities inferred. (b) Locations where the amplification factors: Ψ_x, Ψ_y, f_x^2, f_y^2 are bigger than 1. (c) Velocities associated with the locations shown in panel (b). (d) Velocities that remain after thresholding out points where the amplification factors are larger than one.

Appendix C

Covariance Calculations

Consider the random vector

$$\vec{x} = [x_1 \; x_2 \; x_3 \; \cdots \; x_n]^T \tag{C.1}$$

the elements of which are jointly distributed random variables with

$$E[x_i] = \mu_i \tag{C.2}$$

and

$$cov(x_i, x_j) \equiv E[(x_i - E[x_i])(x_j - E[x_j])] = \sigma_{ij} \tag{C.3}$$

The mean vector is defined to be simply the vector of means

$$E[\vec{x}] = [\mu_1 \; \mu_2 \; \mu_3 \; \cdots \; \mu_n]^T \tag{C.4}$$

The covariance matrix of $\vec{x}$ is defined to be an $n \times n$ symmetric matrix whose ij element, σ_{ij}, is the covariance of x_i and x_j.

Theorem 1. If $\vec{x}$ is a random vector and A a fixed matrix, then

$$cov(A\vec{x}) = Acov(\vec{x})A^T \tag{C.5}$$

Proof: Let's consider the ijth element of the covariance matrix. Since the k element of the vector $A\vec{x}$ is given by

$$(A\vec{x})_k = \sum_{l=1}^{n} a_{kl}x_l \tag{C.6}$$

then, by definition

$$\begin{aligned}
cov(A\vec{x})_{ij} &= cov\left(\sum_{l=1}^{n} a_{il}x_l, \sum_{m=1}^{n} a_{jm}x_m\right) \\
&= E\left[\left(\sum_{l=1}^{n} a_{il}x_l - E\left[\sum_{l=1}^{n} a_{il}x_l\right]\right)\left(\sum_{m=1}^{n} a_{jm}x_m - E\left[\sum_{m=1}^{n} a_{jm}x_m\right]\right)\right] \\
&= E\left[\sum_{l=1}^{n} a_{il}(x_l - E[x_l]) \sum_{m=1}^{n} a_{jm}(x_m - E[x_m])\right] \\
&= \sum_{l=1}^{n}\sum_{m=1}^{n} a_{il}a_{jm}E[(x_l - E[x_l])(x_m - E[x_m])] \\
&= \sum_{l=1}^{n}\sum_{m=1}^{n} a_{il}a_{jm}cov(x_l, x_m) \\
&= \sum_{l=1}^{n}\sum_{m=1}^{n} a_{il}a_{jm}\sigma_{lm} \\
&= \sum_{l=1}^{n}\sum_{m=1}^{n} a_{il}\sigma_{lm}a^T_{mj}
\end{aligned}$$

This is the ijth element of the desired matrix.

Theorem 2. If $\vec{x}$ and $\vec{y}$ are random vectors, then

$$cov(\vec{x} + \vec{y}) = cov(\vec{x}) + cov(\vec{y}) + 2cov(\vec{x}, \vec{y}) \tag{C.7}$$

Proof: Let's consider the ijth element of the covariance matrix:

$$\begin{aligned}
cov(\vec{x} + \vec{y})_{ij} &= E[(x_i + y_i - E[x_i + y_i])(x_j + y_j - E[x_j + y_j])] \\
&= E[(x_i - E[x_i] + y_i - E[y_i])(x_j - E[x_j] + y_j - E[y_j])] \\
&= E[(x_i - E[x_i])(x_j - E[x_j]) + (y_i - E[y_i])(y_j - E[y_j]) + \\
&\qquad (x_i - E[x_i])(y_j - E[y_j]) + (y_i - E[y_i])(x_j - E[x_j])]
\end{aligned}$$

$$= cov(x_i, x_j) + cov(y_i, y_j) + cov(x_i, y_j) + cov(y_i, x_j)$$

$$= cov(x_i, x_j) + cov(y_i, y_j) + 2cov(x_i, y_j)$$

This is the ijth element of the desired matrix.

Theorem 3. If z is a random variable and $\vec{c}$ is a fixed column vector, then

$$cov(\vec{c}z) = \vec{c}\,\vec{c}^T var(z) \tag{C.8}$$

Proof: Let's consider the ijth element of the covariance matrix.

$$\begin{aligned} cov(\vec{c}z)_{ij} &= E[(c_i z - E[c_i z])(c_j z - E[c_j z])] \\ &= c_i c_j E[(z - E[z])(z - E[z])] \\ &= c_i c_j var(z) \end{aligned}$$

This is the ijth element of the desired matrix.

In deriving the results for this appendix, the book by Rice(1988) was very useful.

Appendix D

Divergence – Column Correction

Assuming that $\rho = \rho(z)$, we have that the mass continuity equation becomes

$$\rho \nabla_h \cdot \vec{u} + \frac{\partial}{\partial z}(\rho w) = 0 \tag{D.1}$$

where $\nabla_h \cdot = \hat{\imath}\frac{\partial}{\partial x} + \hat{\jmath}\frac{\partial}{\partial y}$, u and w are the horizontal and vertical velocities, respectively. Integrating D.1 from the surface ($z = 0$) to the top of the cloud system ($z = z_T$), we have

$$\begin{aligned} \int_0^{z_T} \nabla_h \cdot (\rho\vec{u})\, dz &= -\int_0^{z_T} \frac{\partial}{\partial z}(\rho w) dz \\ &= -\left[\rho(z_T) w(x, y, z_T) - \rho(0) w(x, y, 0)\right] \\ &= 0 \end{aligned} \tag{D.2}$$

where we have use the fact that w is zero at the surface and at the top of the cloud system. So, the mass continuity equation does impose a condition on the horizontal mass flux, $\rho\vec{u}$, at every column.

This condition can be broken among other things by errors in measurements as well as for numerical errors after many manipulations of the velocity fields and in particular

when the velocities are subject, for instance, to a smoothing process that brings information from one column to another. In order to restore this basic condition, we use the following procedure. Let $D_u(x,y,z) = \nabla_h \cdot (\rho\vec{u})$ be the uncorrected divergent mass flux. Therefore in general, the vertical integral of D_u will be different than zero and will depend on x and y, i.e.

$$\int_0^{z_T} D_u(x,y,z)dz = C(x,y) \tag{D.3}$$

Since $C(x,y)$ does not depend on z, we can write

$$C(x,y) = \frac{1}{z_T}\int_0^{z_T} C(x,y)\,dz \tag{D.4}$$

Hence, equation D.3 becomes

$$\int_0^{z_T} D_u(x,y,z)\,dz = \int_0^{z_T} \frac{1}{z_T}C(x,y)\,dz \tag{D.5}$$

or

$$\int_0^{z_T} \left[D_u(x,y,z) - \frac{1}{z_T}C(x,y)\right] dz = 0 \tag{D.6}$$

from here, we can define a corrected divergent mass flux as

$$D_c(x,y,z) = D_u(x,y,z) - \frac{1}{z_T}C(x,y) \tag{D.7}$$

or

$$D_c(x,y,z) = \nabla_h \cdot (\rho\vec{u}) - \frac{1}{z_T}\int_0^{z_T} \nabla_h \cdot (\rho\vec{u})\,dz \tag{D.8}$$

Bibliography

[1] Jorgensen D. P. LeMone M. A. and Jou B. J. Precipitation and kinematic structure of an oceanic mesoscale convective system. part i: Convective line structure. *Monthly Weather Review*, **119,**:2608–2637, 1991.

[2] Randy G. Brown and Chidong Zhang. Variability of midtropospheric moisture and its effect on cloud-top height distribution during TOGA COARE. *Journal of the Atmospheric Sciences.*, **54**:2760–2774., 1997.

[3] Herbert B. Callen. *Thermodynamics.* John Wiley & Sons, first edition, 1960.

[4] S. R. de Groot and P. Mazur. *Non-Equilibrium Thermodynamics.* North-Holland Publishing, first edition, 1962.

[5] Richard J. Doviak and Dušan S. Zrnić. *Doppler Radar and Weather Observations.* Academic Press, first edition, 1984.

[6] Kerry A. Emanuel. *Atmospheric Convection.* Oxford University Press, first edition, 1994.

[7] Kerry A. Emanuel, J. David Neelin, and Christopher S. Bretherton. On large-scale circulations in convecting atmospheres. *Quarterly Journal of the Royal Meteorological Society*, **120,**:1111–1143, 1994.

[8] P. Flament and R. Bernstein. Images from the gms-4 satellite during toga-coare (november 1992 to february 1993). Technical report, School of Ocean and Earth Science and Technology, University of Hawaii, Honolulu, Jun 1993. (20 pg, with two CD-ROMs).

[9] Richard H. Johnson, Thomas M. Rickenbach, Steven A. Rutledge, Paul E. Ciesielski, and Wayne H. Schubert. Trimodal characteristics of tropical convection. *J. Climate*, **12,**:2397–2418, 1999.

[10] Houze R. A. Jr. *Cloud Dynamics.* Academic Press, first edition, 1993.

[11] David E. Kingsmill and Robert A. Houze Jr. Kinematic characteristics of air flowing into and out precipitation convection over the west pacific warm pool: An airborne doppler radar survey. *Q. J. R. Meteorol. Soc.*, **125,**:1165–1270, 1999.

[12] López-Cavazos L. *Precipitation development in convective systems over the west Pacific warm pool.* PhD thesis, New Mexico Institute of Mining and Technology, Socorro, NM, 1995.

[13] Kuo-Nan Liou. *An Introduction to Atmospheric Radiation.* Academic Press, first edition, 1980.

[14] C. Lopez-Carrillo and David Raymond. Observational study of tropospheric moisture and deep convection during to ga coare. In *23rd Conference on Hurricanes and Tropical Meteorology*, number JP1.7, 1999.

[15] B.E. Mapes and R.A. Houze Jr. Diabatic divergence profiles in western Pacific mesoscale convective systems. *Journal of Atmospheric Sciences*, **52,**:1807–1828., 1992.

[16] Dimitri Mihalas and Barbara Weibel Mihalas. *Foundations of Radiation Hydrodynamics*. Oxford University Press, first edition, 1984.

[17] I. Prigogine. *Thermodynamics of irreversible processes*. John Wiley & Sons, third edition, 1955.

[18] D. J. Raymond. Regulation of moist convection over the west Pacific warm pool. *Journal of Atmospheric Sciences*, **15,**:3945–3959., 1995.

[19] D. J. Raymond and S. A. Lewis. Rotating convective disturbances in the trades. *Quart. J. Roy. Meteor. Soc.*, **121,**:271–299., 1995.

[20] D. J. Raymond, C. López-Carrillo, and L. López Cavazos. Case studies of developing east Pacific easterly waves. *Quart. J. Roy. Meteor. Soc.*, **124**:2005–2034, 1998.

[21] John A. Rice. *Mathematical Statistics and Data Analysis*. Wadsworth & Brooks, first edition, 1988.

[22] Steven C. Sherwood. Convective precursors and predictability in the tropical western Pacific. *Mon. Wea. Rev.*, 127:2977–2991, 1999.

[23] Peter J. Webster and Roger Lukas. TOGA COARE : The coupled ocean-atmosphere response experiment. *Bulletin American Meteorological Society*, **73,**:1377–1416., 1992.